PHENIX Beam Use Proposal
for
RHIC Run-13 and Run-14

The PHENIX Collaboration

May 30, 2012

1 Executive summary

The main goals for PHENIX in Run-13 and Run-14 are to make definitive measurements utilizing our recently upgraded detector capabilities. These include the Muon Trigger system, which was fully installed for Run-12, the silicon vertex detectors VTX and FVTX, which were installed before Run-11 and Run-12, respectively, and the new MPC-EX, a preshower detector located in front of the Muon Piston Calorimeter which will separate direct photons from neutral meson decays. Installation of the MPC-EX is anticipated prior to Run-14.

Our highest priority for Run-13 is to complete the W physics program by finishing accumulation of a large 500 GeV polarized $p+p$ collision data set. We measure single-spin asymmetries of W bosons in the forward and backward directions, as well as at midrapidity, to determine light anti-quark polarizations. The measurement requires 300 pb^{-1} sampled; 50 pb^{-1} have been collected to date. Collecting the remainder of the data in Run-13 will allow us to meet key milestones in time. NSAC milestone HP8 to measure flavor-identified q and $\bar{q}$ contributions to the spin of the proton via the longitudinal spin asymmetry of W production is due in 2013. The RIKEN W physics milestone in Japan is

for 2014. In addition, completing the long longitudinally polarized 500 GeV $p+p$ run reduces pressure on future Runs, which is important given the reduced number of cryo weeks anticipated. This goal will require 13-14 weeks, i.e. potentially all of Run-13. Should there be cryo weeks in addition to the baseline plan of 15 weeks, we anticipate that at least some of the additional time will be needed to reach our integrated luminosity goal for 500 GeV $p+p$.

Our second priority for Run-13, should there be additional cryo weeks and the 500 GeV $p+p$ goal is reached, is to sample 5.5 pb^{-1} of 200 GeV $p+p$ with collision vertex inside $\pm$ 10 cm. We estimate that this requires 29 pb^{-1} delivered. These data will provide comparison data for the FVTX heavy flavor physics program. Transverse polarization in this run will allow adding statistics to the Run-12 A_N measurements with the MPC. The desired physics performance requires adding 16 pb^{-1} in $\pm$ 30 cm to existing data sets, i.e. 42 $pb-1$ delivered in Run-13. Based upon CA-D luminosity estimates, we anticipate that collecting the integrated luminosity for both measurements will require approximately 4 weeks, including the energy change. FVTX physics, with lower quality MPC measurements, could be achieved in approximately 3 weeks. Should completion of the 500 GeV $p+p$ leave fewer than 3 weeks, we request $p+p$ comparison running at 39 GeV, as detailed in Section 5.

For Run-14, our highest priority is 200 GeV Au+Au for heavy flavor physics with the FVTX. This also utilizes the fully instrumented VTX, as all repaired ladders will be installed into the VTX prior to Run-14. The physics goals call for 0.8-1.0 nb^{-1} sampled inside $\pm$ 10 cm. This will require 6-8 weeks of Au+Au collisions, during which we expect 5-7.5 nb^{-1} delivered by RHIC.

Our second priority for Run-14 is to collect the 200 GeV $p+p$ sample described above, should that not have already been accomplished in Run-13. Our third priority for Run-14 is to begin the measurement of the nuclear parton distribution functions at small x using direct photons measured in the MPC-EX. There is an ongoing discussion as to whether this is best achieved with p+Au or d+Au collisions, described more in Section 5 below. However, an initial d+Au run in 2014 would allow a first look with the MPC-EX, along with a first measurement of cold nuclear matter effects upon open heavy flavor and quarkonia production using the FVTX plus PHENIX muon arms.

The PHENIX beam use proposal for Run-13 and Run-14, in order of priority, is as follows.

15+5 cryo-week proposal for Run-13:

1. 500 GeV $p+p$ for 10 weeks

2. 500 GeV $p+p$ for 1-5 additional weeks, if needed to reach 250 pb^{-1} sampled inside $\pm$ 30 cm

3. 200 GeV $p+p$ if 3-4 weeks remain following the 500 GeV run

4. if fewer than 3 weeks remain following the 500 GeV Run, we request 4.2 pb^{-1} delivered of 39 GeV $p+p$ ($\approx$ 1 week)

15+5 cryo-week proposal for Run-14, assuming 200 GeV $p+p$ is done

in Run-13:

1. 200 GeV Au+Au for 6-8 weeks, to collect 1 nb^{-1} in $\pm$ 10 cm

2. 200 GeV d+Au for the remainder of the Run

15+5 cryo-week proposal for Run-14, assuming no 200 GeV $p+p$ in Run-13:

1. 200 GeV Au+Au for 6-8 weeks, to collect 1 nb^{-1} in $\pm$ 10 cm

2. 200 GeV $p+p$ for 4 weeks

3. 200 GeV d+Au for the remainder of the Run

NB: This is a priority-ordered list. Clearly, $p+p$ in the middle does not correspond to an optimum ordering of species. The actual order of beam species to follow the Au+Au should be determined with CAD, STAR, and the ALD, once the boundary conditions defined by run lengths and the species studied in Run-13 are known.

2 Introduction

The PHENIX Collaboration is pursuing a scientific program of precision measurements to address compelling questions on the formation, evolution, and properties of the quark-gluon plasma, and to measure the spin structure of the proton. Our approach is to simultaneously collect data, analyze and publish physics results, while at the same time pursuing a vigorous program of upgrades. The upgrades ensure that the PHENIX capabilities evolve as we better understand the physics, and allow us to take advantage of improved accelerator luminosities, polarization, and reach in beam species. As PHENIX was designed with high rate capability and selective triggers, a consistent theme is the need for the highest possible integrated luminosities and proton beam polarization.

Our ambitious upgrade program has put into place

- A trigger for high momentum muons from *W* decays, completed for Run-12

- Silicon microvertex barrel detector, VTX, completed for Run-11

- Forward silicon microvertex detector, FVTX, completed for Run-12

- Ongoing, incremental improvements in the DAQ system to maintain high rate while accommodating the additional data volume from new detectors. These improvements are collectively known as DAQ2010

- A proposal to instrument the muon piston calorimeter with a Si/W preshower detector, MPC-EX, in time for Run-14

We applaud the recent CA-D successes with stochastic cooling of heavy ion beams, improved polarization, and ongoing implementation of electron lenses to increase the $p+p$ collision luminosity. This Beam Use Proposal is designed to take full advantage of the improved collider capabilities and fully utilize the PHENIX upgrades to meet international milestones for RHIC science. Though serious challenges are presented by curtailed run lengths, the plan we present is designed to deliver key physics goals on time.

These goals include

- Definitive measurement of the W asymmetries in Run-13. This drives the request for a dedicated 500 GeV $p+p$ run to sample integrated luminosity of 250 pb^{-1}, and addresses NSAC milestone HP8 (due in 2013) and the Japanese W milestone due by 2014.

- Measurement of the rapidity dependence of charm and bottom energy loss in Au+Au collisions, utilizing the VTX and FVTX. This requires a long 200 GeV Au+Au run in Run-14, and a 200 GeV $p+p$ comparison run in Run-13 or 14. These Runs comprise the first step toward addressing NSAC milestone DM12, to be completed by 2016.

- Completing measurements of the transverse polarization, A_N, of neutral pions at forward rapidity. Consequently, we request transverse polarization of the proton beams for the 200 GeV running.

- Utilization of direct photons at forward rapidity to probe gluon shadowing and/or saturation at small-x in heavy nuclei. This necessitates installation and commissioning of the MPC-EX in Run-14. Should the 200 GeV $p+p$ be part of Run-14, this would begin accumulation of large data sets with the MPC-EX. The measurement requires approximately 12 weeks p+Au (or d+Au) collisions in Run-15, along with a commensurate sample of $p+p$ collisions for comparison. The measurement will address NSAC milestone DM8.

The 500 GeV $p+p$ in Run-11 presented challenges due to the low luminosity and insufficient polarization. The performance in Run-12 was much more encouraging, thanks to hard work and creative developments by CA-D. The improved polarization and daily integrated luminosity reached after ramp-up implies that the bulk of the required data set can be collected in one long 500 GeV polarized proton Run. However, this will require a somewhat different running mode. Instead of halting data taking for APEX and/or machine development and/or maintenance weekly, it is necessary to plan two-week periods of continuous data-taking. Doing otherwise poses an unacceptably high risk of missing the W physics goals. In these times of shortened annual running periods, other pressing priorities imply that we will be unable to return to 500 GeV $p+p$ for several years. Consequently, we must ensure sufficient statistics in Run-13. More details are given below, in the section outlining the assumptions in our beam use request.

3 Recent scientific accomplishments

The papers submitted, or about to be submitted, for publication over the past year generally fall into one of several themes. PHENIX continues to exploit electromagnetic probes of the quark-gluon plasma, with new results on direct photon spectra, nuclear modification (or not), and flow [15]. We analyze photon production utilizing three different techniques, and study photons in Au+Au, d+Au and p+p collisions [1, 2, 3].

PHENIX has measured jet fragmentation functions using direct photons to tag the jet energy [4]. We have also undertaken a detailed study of jet modification as a function of the trigger jet orientation with respect to the reaction plane.

A key thrust for PHENIX has been to understand the formation of heavy flavor bound states and the suppression of J/ψ in quark gluon plasma. Color screening is one of the oldest predicted signatures of quark-gluon plasma, but experimental and theoretical study of this have been fraught with various complications. The beam energy dependence of the observed suppression is quite mysterious. This indicates that quantifying the screening in the plasma requires understanding of initial state effects on heavy flavor formation, cold nuclear matter effects upon the probability that heavy $q\bar{q}$ pairs remain bound, and final state effects such as regeneration of bound states when copious heavy q and $\bar{q}$ are present.

PHENIX has published a new high statistics measurement of J/ψ in Au+Au, in an archival paper [16]. Nuclear effects on heavy flavor bound state survival are quantified using the rapidity and p_T dependence of J/ψ, and v in d+Au collisions [19, 5]. We have also published the spectra of $\psi\prime$ and χ_C in p+p collisions [21]. Disentangling initial and final state hot and cold nuclear matter suppression of bound states is further aided by new measurements of R_{dA} for semileptonic decays of D and B mesons at forward and central rapidity [14, 6]. In addition, we have published a highly anticipated measurement of nuclear effects upon the partonic structure of nucleons via correlations of forward-going particles [20].

PHENIX utilizes the RHIC energy scan data in several ways. We will soon submit a publication on the $\sqrt{s}$ dependence of particle and energy flow fluctuations [7]. In order to explore the temperature dependence of plasma properties such as opacity, color screening, and η/s, we have studied the $\sqrt{s}$ dependence of π^0 [13] and J/ψ [8] production, as

6

well as the elliptic flow of different mass hadrons [12].

Recent results on the spin of the proton include A_{LL} for charged hadrons [11] and transverse single spin asymmetries for neutral hadrons at forward rapidity [9]. Analysis of W production from the Run-11 data set is underway, and work to prepare reconstruction of the Run-12 500 GeV $p+p$ data is ongoing.

3.1 Direct photon recent highlights

Direct, i.e. nondecay, photons are excellent probes of the quark-gluon plasma. As they interact only electromagnetically, photons preserve information from early stages in collision, and allow a glimpse of the early dynamics. Direct photons with intermediate and high transverse momenta ($p_T > 4$ GeV/c) are produced predominantly in initial hard scattering of the colliding quarks and gluons, such as $q + g \rightarrow q + \gamma$ or $q + \bar{q} \rightarrow g + \gamma$. In addition, they can be produced as bremsstrahlung emitted by a scattered parton from the fragmentation of quarks and gluons, or from the interaction of a parton with the medium created in heavy-ion collisions. Lower p_T photons can be emitted as thermal radiation from the partonic and hadronic phases. Last year, PHENIX reported that thermal photons exhibit a surprisingly high collective flow. This result has recently been confirmed by detection of electron-positron pairs from conversions of low momentum photons.

Direct photon cross sections and spectra can be affected by modification of the initial state in the colliding nuclei, for example by shadowing or anti-shadowing of the partons. The different isospin composition of Au nuclei as compared to protons may also be important, as the different quark content of p and n should influence the yield of photons from initial hard scatterings. Such effects can be searched for by measuring the nuclear modification factor, R_{AA} for direct photons over a large p_T range. This factor is defined as

$$R_{AA}p_T = \frac{(1/N_{AA}^{evt})d^2N_{AA}/dp_Tdy}{<T_{AA}> \times d^2\sigma_{pp}/dp_Tdy},$$
(1)

where $<T_{AA}>$ is the average nuclear thickness function and $d^2\sigma_{pp}/dp_Tdy$ is the measured $p+p$ cross section.

R_{AA} was constructed for direct photons using new, high quality measurements of the

direct photon spectrum in $p+p$[1] and Au+Au[2] collisions. We found that the nuclear modification factor is consistent with unity for all centrality bins over the entire p_T range up to 22 GeV/c. Figure 4 shows the direct photon R_{AA} for the 0-5% most central collisions; error bars show point-to-point uncertainties including statistical errors, while the boxes depict p_T correlated systematic uncertainties. The dark gray box on the left shows the uncertainty on the total inelastic $p+p$ cross section, while the dark box on the right shows the uncertainty in N_{coll}.
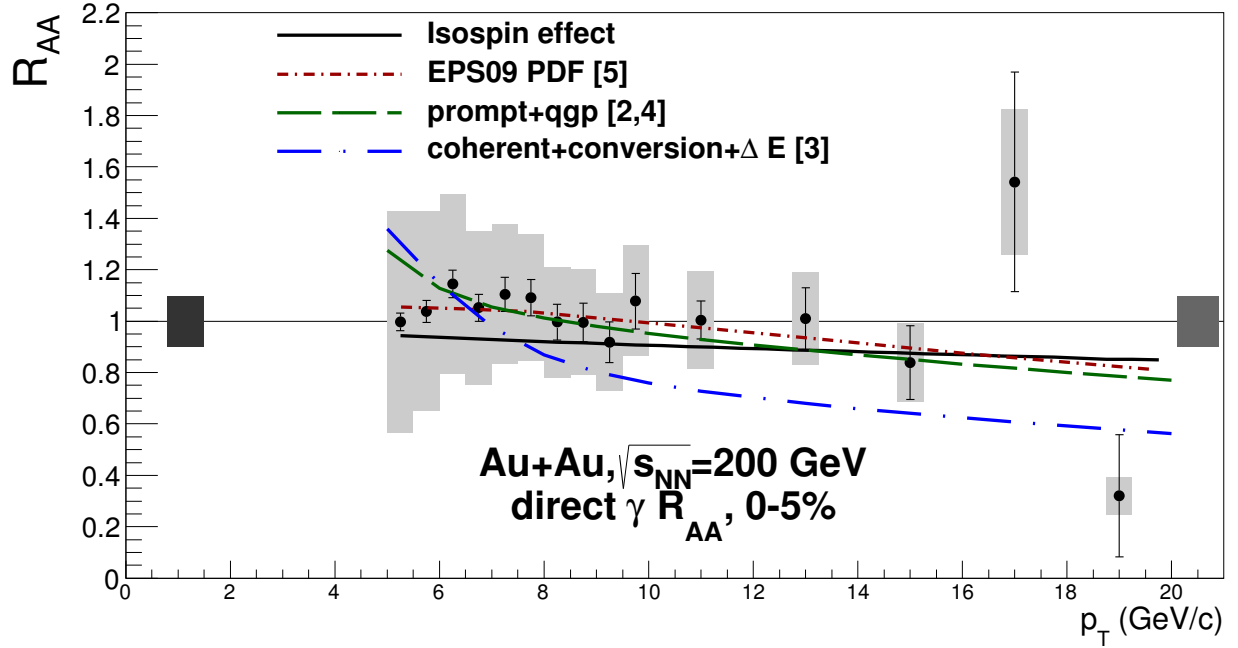
Figure 1: Direct photon nuclear modification factor for 0-5% most central events[2], compared with theoretical calculations for different scenarios. See text for details and references.

No evidence is seen of an isospin effect, but other physics may pull the ratio in the opposite direction. Figure 1 compares the data to theoretical models including various initial state and final-state effects [37, 39, 33, 25]. Initial state effects include the isospin effect arising from different photon cross sections in $p+p$, n+n, and p+n collisions (curve labeled "Isospin effect" in Fig. 1), and modifications of nuclear structure functions due to shadowing and anti-shadowing of partons (EPS09 PDF) [25]. The EPS09 calculation also includes the isospin effect. Final state modifications in the QGP lead, on one hand, to decreased photon yield, since energy loss of a parton also means suppression of the corresponding fragmentation photons. On the other hand, increase direct photon yield is predicted due to radiation resulting from jet-medium interactions ("prompt+QGP") [37, 33]. This final state calculation also takes into account the aforementioned initial state effects. Another calculation[39] includes initial state effects, as

well as final state energy loss, medium-induced photon bremsstrahlung, and the LPM effect ("coherent+conversion+E").

The data are consistent with a scenario where hard scattered photons simply traverse the matter unaffected, as well as with the isospin effect plus modifications of the nuclear PDFs. Balancing effects from the QGP such as fragmentation photon suppression and enhancement due to jet-medium interactions are not excluded by the data. The approach in [39] is in disagreement with the data. This confirms that the majority (if not all) direct photons at high p_T come directly from hard scattering processes and suggests that possible effects from the QGP all but cancel.

3.2   Heavy flavor

In the past year we completed two archival papers on J/ψ production, in Au+Au and d+Au collisions. Figure 2 shows the nuclear modification factor for J/ψ measured at midrapidity in the central arms and at rapidity $1.2 < |y| < 2.2$ from the muon arms. The statistical precision of the newly published 2007 data set [19] is greatly improved. It is clear that J/ψ are significantly more suppressed at forward than at midrapidity.

Detailed comparison of the centrality, p_T, and rapidity dependence to predictions of models including various cold nuclear matter effects shows that the suppression is attributable to hot nuclear matter effects [19]. Some of these models include only initial state effects, while others also include final state effects, but none is able to reproduce the Au+Au data on its own.

Initial nuclear wave functions described by the Color Glass Condensate result in suppression of J/ψ production and narrowing of the rapidity distribution due to saturation of the gluon fields in heavy ion collisions compared to p+p [35]. This model, with a free parameter for suppression in central Au+Au collisions due to hot matter effects, reproduces the suppression trend between mid and forward rapidity. It is notable that the suppression is essentially independent of Au+Au centrality in this model, whereas the data show the suppression factor approaching one in the most peripheral events. Furthermore, coherence of double gluon exchange in this picture implies an enhancement in d+Au collisions at midrapidity, which is not observed [18].
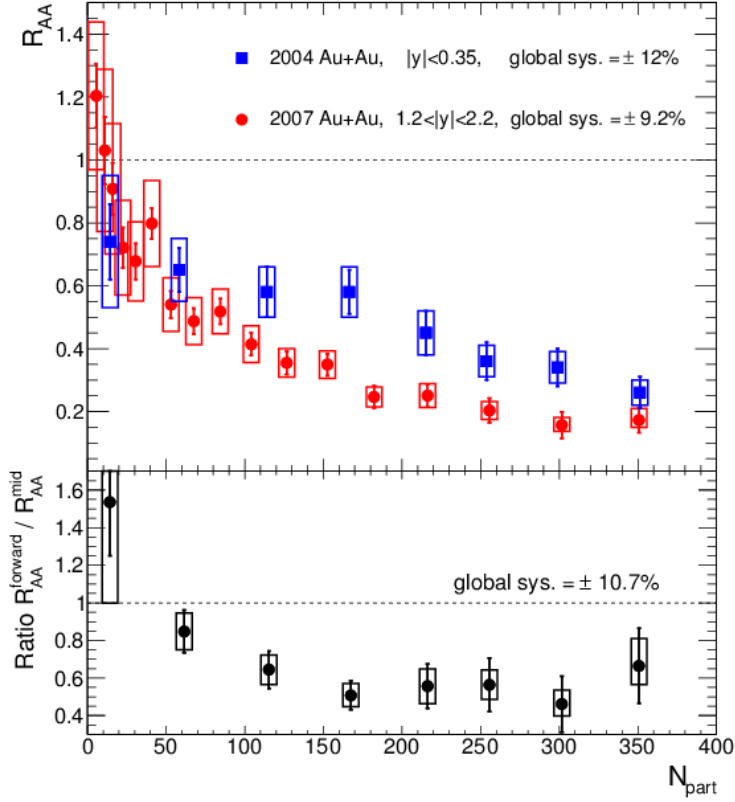
Figure 2: The R_{AA} for J/ψ, as a function of N_{part}, at two rapidities. The forward rapidity points show newly published 2007 data [19]. The lower panel provides the ratio of forward to midrapidity J/ψ production.

Accounting for J/ψ breakup by interaction with a dense co-moving final-state medium [29, 28]. does not reproduce the observed J/ψ dependence on rapidity and $\sqrt{s}$ of heavy ion collisions. Cold nuclear matter effects such as nuclear shadowing and nuclear absorption are much stronger at forward than midrapidity. On the other hand, the effects of comover dissociation (and regeneration) are stronger at midrapidity. The combination of these effects leads to a predicted suppression that varies little with rapidity, in disagreement with the data.

Shown in Fig. 3 are new results for the p_T dependence of J/ψ at forward rapidity along with the previously published 2004 midrapidity results. As there has been much recent interest in whether the R_{AA} as a function of p_T rises or falls, we performed a simple linear fit to the R_{AA} at forward rapidity over the full p_T range [19]. Only the 20-40% centrality bin has a statistically significant increase in R_{AA} with p_T. This does not agree
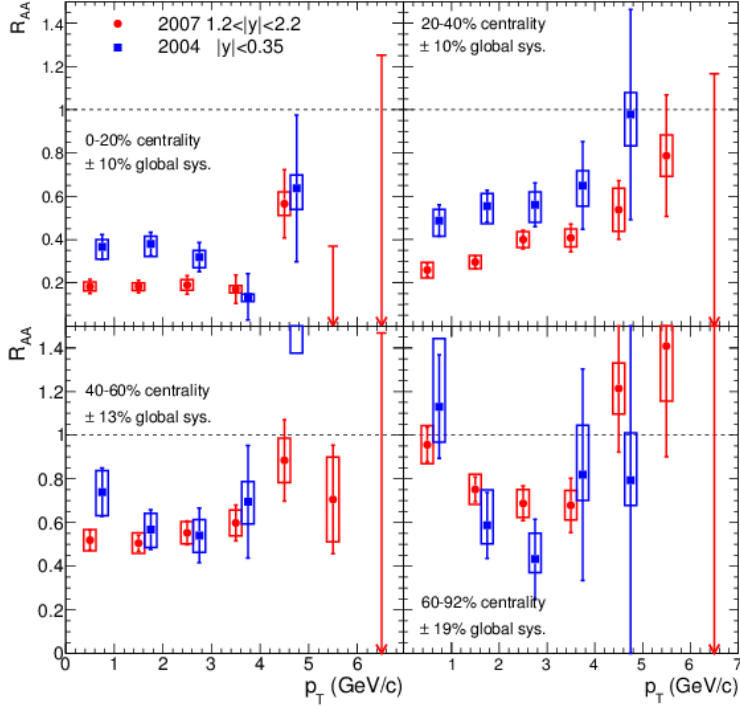
Figure 3: $J/\psi R_{AA}$ as a function of p_T in four centrality bins in Au+Au collisions [19]

with predictions of the Hot Wind model [36], although the model predictions are for mid rather than forward rapidity, where the statistical precision of our data is best. The observed p_T dependence can be reproduced by Zhao and Rapp [42]. They include various initial state, final state and feed-down effects as well as allowing for a rapidity dependent J/ψ breakup cross section and regeneration of J/ψ by final state coalescence of $c\bar{c}$ pairs. Clearly, extracting the magnitude of the hot matter suppression requires good control of all of these effects.

Consequently, we have continued to extract physics from the rich d+Au data set collected in Run-8. Our approach is to carry out systematic, high precision studies of quarkonium and open heavy flavor production as a function of rapidity, p_T, and d+Au collision centrality. We have also published the spectra of $\psi\prime$ and χ_C in p+p collisions, which provide a baseline for measurements with heavy ions [21]. Effects on heavy flavor bound state survival of cold nuclear matter and of a dense co-moving final state medium are quantified using the rapidity and p_T dependence of J/ψ, and v in d+Au collisions [16, 5].

We observe that that the nuclear modification is largest for collisions with small impact
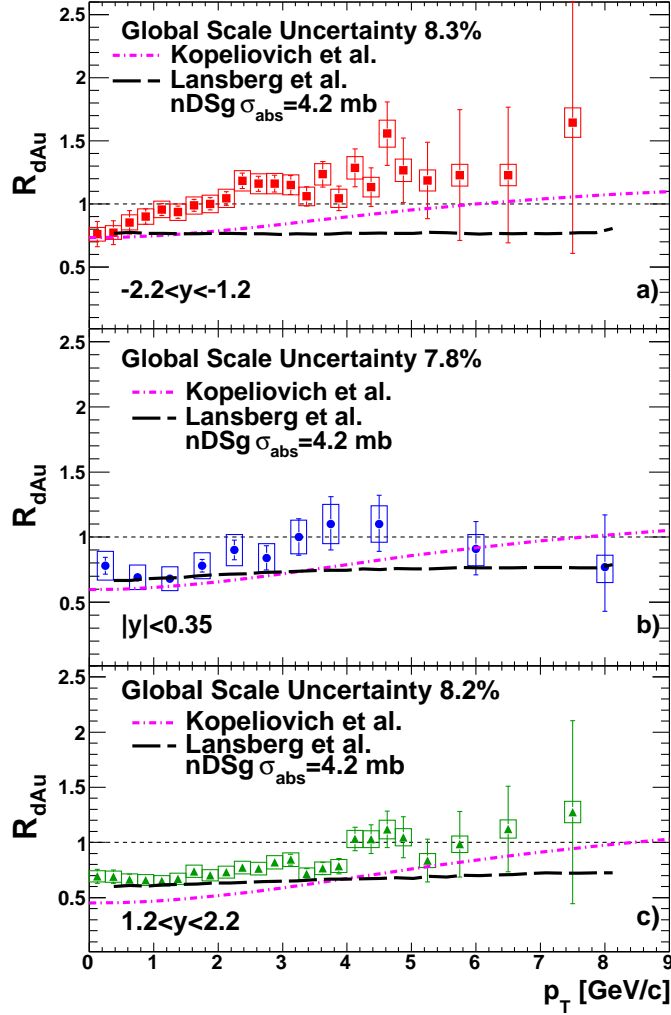
Figure 4: J/ψ nuclear modification, R_{dAu} as a function of p_T for (a) backward rapidity, (b) midrapidity, and (c) forward rapidity in centrality integrated d+Au collisions. Curves correspond to model predictions discussed below. [16]

parameter. Figure 4 shows suppression of J/ψ for $p_T < 4$ GeV/c at positive rapidity. At negative rapidity J/ψ is suppressed for $p_T < 2$ GeV/c then enhanced for $p_T > 2$ GeV/c [16]. At mid and forward rapidity, the average R_{dAu} for $p_T > 4$ GeV/c is consistent with 1.0, while at backward rapidity it is greater than 1.0. We note that the measured J/ψ at backward rapidity probe the gluon distribution in the Au nucleus in a range of roughly $0.051 < x < 0.39$, assuming simple 2→1 kinematics. The forward rapidity J/ψ cover approximately $0.0017 < x < 0.013$. The $\Delta < p_T^2 >$ values determined from the data show a marked increase with N_{coll} that is similar at all rapidities [16].

12

Models aiming to describe these data include various combinations of cold nuclear matter effects including shadowing, nuclear breakup, and the Cronin effect. There are a number of nuclear PDF sets available, which are based upon various parameterizations of the available data. At mid and forward rapidity, calculations using the different nPDFs and different shadowing and Cronin effects can reproduce the p_T and centrality dependence of the measured R_{dAu}. However, they have more difficulty at backward rapidity in all but the most peripheral collisions, where data and calculations agree that R_{dAu} is consistent with 1.0 at all p_T. The precision and p_T reach of these new data not only help pin down the nuclear breakup cross section, they also provide new constraints on nuclear modification of gluon distributions and the magnitude of the Cronin effect on J/ψ production at RHIC energy.

Disentangling initial and final state nuclear suppression of bound states, along with pinning down cold nuclear matter effects on heavy flavor suppression, is aided by new measurements of R_{dA} for semileptonic decays of D and B mesons at forward and central rapidity [14, 6].

PHENIX has also looked at the behavior of hard probes at a function of the RHIC collision energy. Figure 5 shows one measure of the nuclear modification factor, R_{CP}, for $J/\psi \rightarrow \mu^+\mu^-$ in Au+Au collisions at $\sqrt{s_{NN}} = 200$, 62.4 and 39 GeV. Comparing the results at lower energies, one sees that they are consistent with the results from full energy RHIC collisions. The production of quarkonia is one of the most durable puzzles of high energy collision and these results add to the growing encyclopedia of data that will help resolve this mystery. It should be noted, however, that a more quantitative study of the $\sqrt{s}$ dependence of J/ψ suppression will require $p+p$ reference data so that we may determine R_{AA} instead of relying upon the central to peripheral collision yield ratio. Ultimately, d+Au running at lower energy will also be required, in order to disentangle cold nuclear matter effects from suppression in quark-gluon plasma. We anticipate requesting this in Run-14.
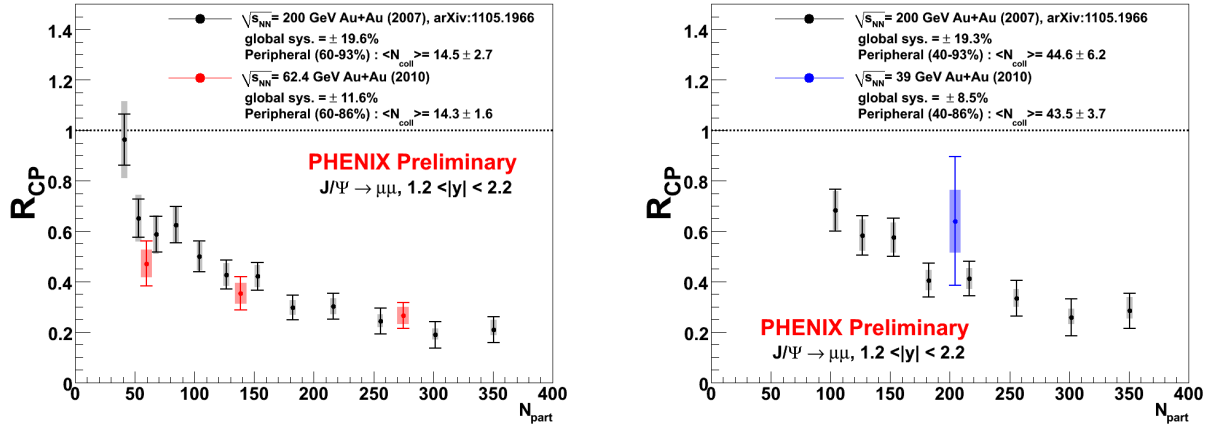
Figure 5: R_{CP} for J/ψ as measured in Au+Au collisions at $\sqrt{s_{NN}} = 200, 62.4$ and $39\,\text{GeV}$

3.3 Global Variables from the RHIC Beam Energy Scan

3.3.1 Charged Particle Multiplicity and Transverse Energy Production

During Run-10 and Run-11, RHIC provided Au+Au collisions at a variety of energies in order to probe different regions of the QCD phase diagram. One goal of this program is to search for signatures of the existence of a critical point. In Run-10, PHENIX recorded 700 million events at 62.4 GeV, 250 million events at 39 GeV, and 1.5 million events at 7.7 GeV. In Run-11, PHENIX took 44 million events at 27 GeV and 13 million events at 19.6 GeV.

PHENIX has measured the charged particle multiplicity, $dN/d\eta$ and the transverse energy production, $dE_T/d\eta$, at 62.4, 39, 19.6, and 7.7 GeV. Figure 6 shows $dE_T/d\eta$ normalized by the number of participant pairs as a function of centrality for Au+Au collisions at 7.7 GeV and 200 GeV compared to Pb+Pb collisions at 2.76 TeV. There is no change in the centrality-dependence over this energy range. The excitation function for dN_{ch}/dy per participant pair in central collisions is shown in Fig. 7.

The Bjorken energy density can be estimated as follows:

$$\epsilon_{BJ} = \frac{1}{A_\perp \tau} \frac{dE_T}{dy}, \tag{2}$$
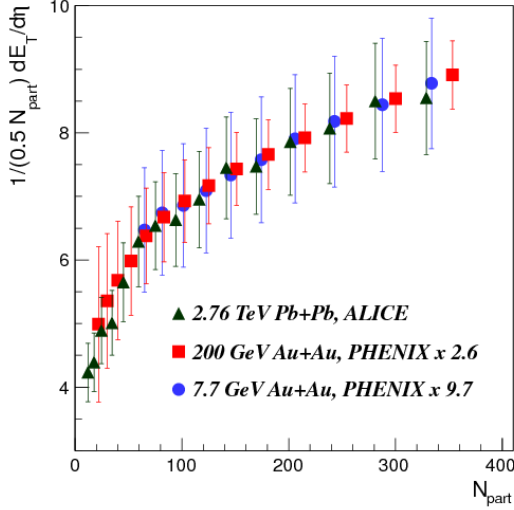
14

Figure 6: $dE_T/d\eta$ normalized by the number of participant pairs as a function of N_{part} for 2.76 Pb+Pb, 200 GeV Au+Au, and 7.7 GeV Au+Au collisions. The PHENIX data has been scaled up for comparison to the 2.76 TeV Pb+Pb data.
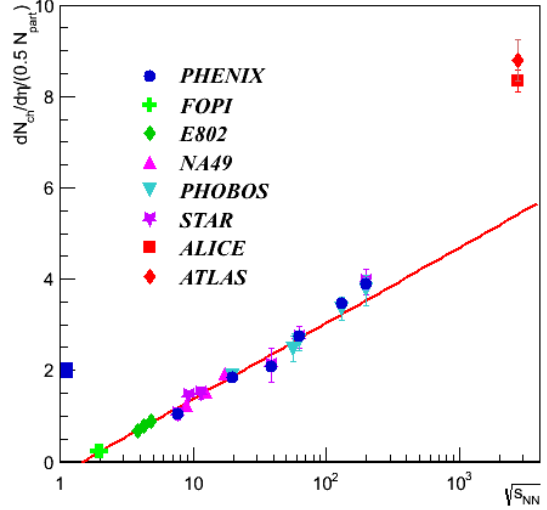
Figure 7: $dN_{ch}/d\eta$ normalized by the number of participant pairs for central events as a function of $\sqrt{s_{NN}}$. The red line is an exponential fit to the data excluding the ALICE and ATLAS data points.

where $A_\perp$ is the transverse overlap area of the nuclei determined from the Glauber model, and τ is the formation time. The value of $dE_T/d\eta$ is multiplied by a factor of 1.25 to obtain dE_T/dy at the SPS energies. The excitation function of the Bjorken energy density for central collisions is shown in Fig. 8. Note that for the most central collisions at 7.7 GeV, the Bjorken energy density is $1.44 \pm 0.11 GeV/fm^3$, above the value of 1.0 for a formation time of 1 fm/c, which is the QGP formation threshold in Bjorken's original paper [27].

3.3.2 Net Charge Fluctuations

PHENIX has measured the skewness and kurtosis of distributions of the net charge in Au+Au collisions at 7.7, 39, 62.4, and 200 GeV. The correlation length ξ, which should diverge at the critical point, is related to moments of conserved quantities including the net charge. The skewness is expected to scale as $\xi^{4.5}$ and the kurtosis is expected to scale as ξ^7, so these observables are sensitive to the presence of a critical point. The skewness and
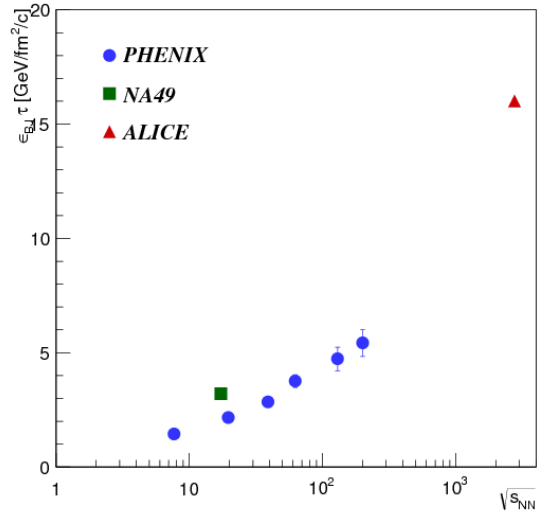
15

Figure 8: The estimated Bjorken energy density multiplied by the formation time as a function of $\sqrt{s_{NN}}$.
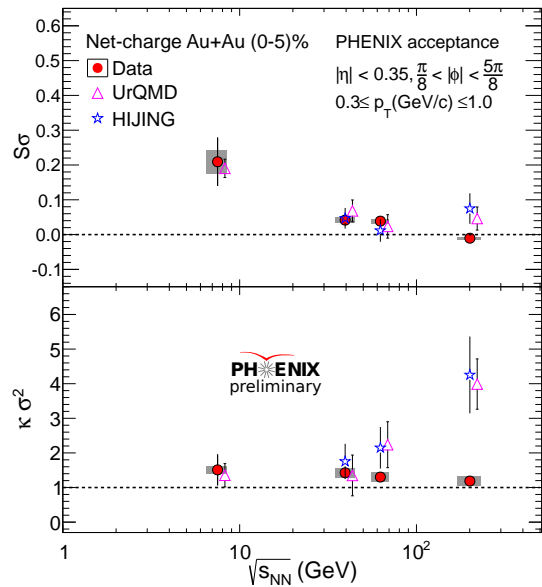

Figure 9: The skewness and kurtosis of the net charge distribution as a function of $\sqrt{s_{NN}}$. Also shown are comparisons to simulations from the URQMD and HIJING models in the PHENIX acceptance.

kurtosis are shown in Fig. 9, compared to predictions of the HIJING and URQMD model. No excess fluctuations in the net charge are observed. Experience from PHENIX measurements has shown that an analysis of baseline $p+p$ results at each energy is extremely useful for interpretation of fluctuation results.

4 Upgrades Accomplishments

4.1 Forward Vertex Detector (FVTX)

The two Forward Silicon Vertex Trackers (FVTX) for the PHENIX experiment extend the vertex capability of the PHENIX Silicon Vertex Tracker (VTX) to forward and backward rapidities, providing space points before the absorber and secondary vertex measure-

16

ment capability in front of the PHENIX muon arms. The FVTX detector was successfully installed into PHENIX in December 2011 and has undergone commissioning and operations during the 2012 Run. 200 GeV $p+p$ was largely used for commissioning, along with part of the 200 GeV U+U collision running. The FVTX collected a good $p+p$ 510 GeV data set, a sample of U+U data and is currently recording Cu+Au data together with the rest of the PHENIX detector.

The FVTX was installed to identify secondary vertices near the original event vertex. With an expected distance of closest approach (DCA) resolution of 200 μm or better at 5 GeV/c, we will be able to separate prompt particles from particles that have short decay distances (B and D mesons) and longer-lived particles such as pions and kaons. The FVTX detector will also improve the dimuon mass resolution by providing a better opening angle measurement than can be provided by the muon arms, will allow for isolation cuts to help discriminate between muon signals and hadronic backgrounds, and will provide further discrimination against hadronic particles which decay in the muon volume by requiring that the track passing through the FVTX planes and the muon planes have a good chi-square fit value.

A picture of the completed FVTX detector, integrated with the VTX detector, can be seen in Fig. 10. Q/A studies showed that 99.9% of sensor channels and readout were functional. However, during the installation and commissioning process two readout boards were damaged, and two data fibers were not connected due to interference with a preexisting support structure. Consequently, approximately 90% of the detector is operational.
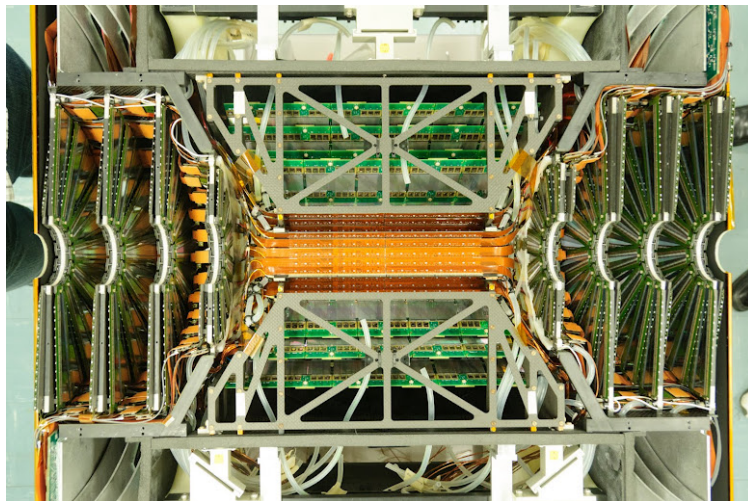

Figure 10: One half of the integrated FVTX and VTX detectors.

The performance of the FVTX detector has been studied using real collision data and front-end injection calibration data. All detector performance specifications have been met, including >95% detector efficiency in the active area, ∼500 electrons noise level on all readout channels, and intrinsic detector resolution limited only by the readout pitch and multiple scattering of particles. We have also established that our coordinate calculations and track finding algorithms work and that we can correlate tracks in the FVTX with the BBC and VTX vertex positions and with tracks from the Muon Arms. We are currently incorporating all FVTX survey information into the analyses and refining the alignment using straight tracks.

The noise and threshold values measured during a typical calibration run can be seen in Fig. 11 (left). Also shown is an extracted track residual for our third station. The extracted value of ≈ 48 μm agrees very well with simulations of expected detector performance with a strip pitch of 75 μms, and averaging over the momentum of tracks populating the FVTX detector.
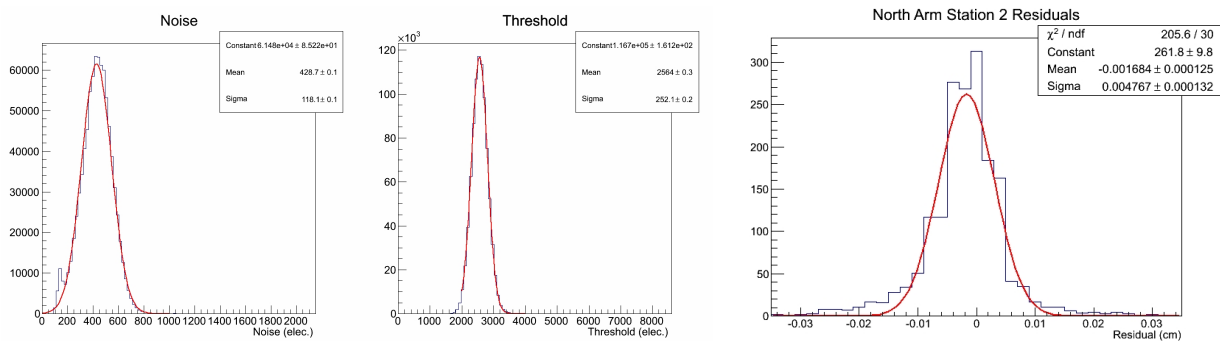

Figure 11: The (left-most) noise and (middle) threshold values for each of our silicon readout channels are extracted from calibration data. We extract mean values of ≈ 430 electrons noise and ≈ 2500 electrons threshold value, which compares well with our specification to have ≈ 500 electrons noise. The right-most panel shows the third station track residuals.

Figure 12 shows reconstructed events in the FVTX. The left panel shows a relatively clean $p+p$ event with two apparent back-to-back tracks reconstructed. The right panel shows a much busier U+U event with all the reconstructed tracks projected to the primary collision position in Z (the beam direction).
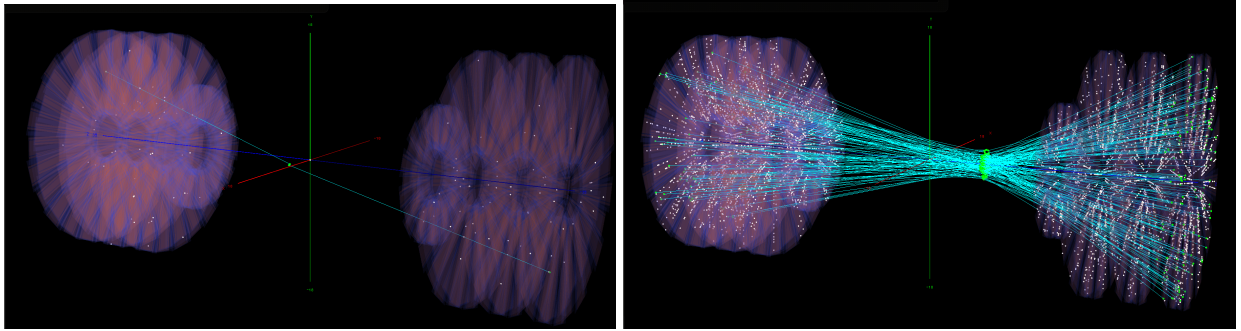
Figure 12: Two reconstructed events in the FVTX detector: the left-side panel is a $p+p$ event and the right-side panel shows a U+U event. The silicon detector wedges are visible in pink/blue, while lines show the tracks of particles traversing multiple FVTX layers.
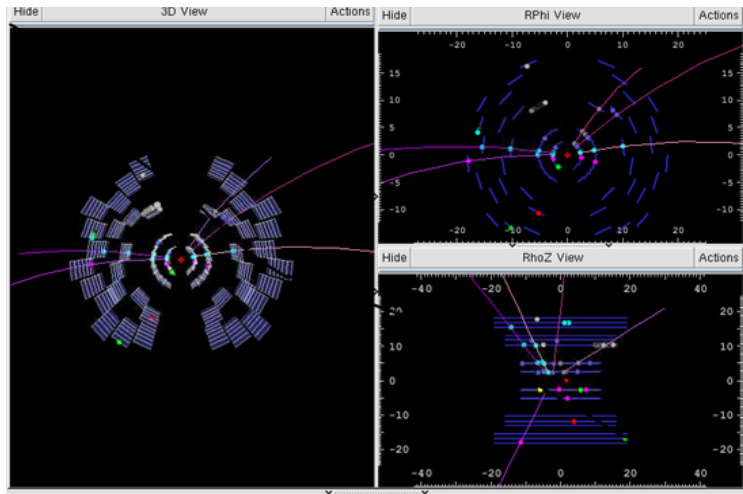

Figure 13: Example of VTX event display of a 500 GeV $p+p$ collision in Run-12.

4.2 Vertex Detector (VTX)

The barrel silicon microvertex detector, VTX, is also visible in Fig. 10. The VTX consists of two layers of pixel sensors, surrounded by two layers of stripixels. It was installed in PHENIX prior to Run-11, and was commissioned during last year's proton running. We collected approximately 3.4B events with the VTX during the 200 GeV Au+Au in Run-11. These data are currently being analyzed. The VTX has collected data during all of Run-12. Fig. 13 shows a sample event display from the Run-12 500 GeV $p+p$ data.
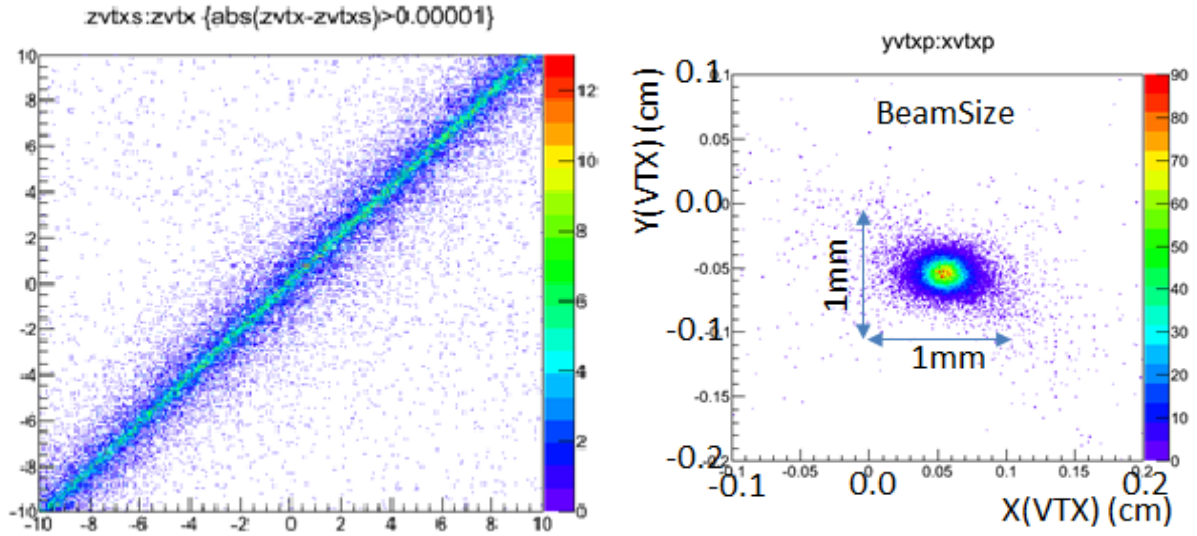
Figure 14: Event vertex Z position reconstructed by BBC vs event vertex Z position reconstructed by VTX (left). Beam spot size reconstructed by VTX (right).

The main purpose of the VTX is to identify the displaced vertices of D and B meson decays, allowing separate identification of open charm and open beauty. The VTX also provides large solid angle stand-alone tracking, albeit with modest momentum resolution ($\delta p/p \simeq 5\% \oplus 10\%p$). This will nevertheless improve jet and hadron flow measurements in PHENIX. Furthermore, the VTX detector provides an accurate measurement of the event vertex; the precision of a few tens of microns is much higher than is achievable with the beam-beam counter (BBC) arrays. Lastly, the VTX provides an independent measurement of the reaction plane (i.e. direction of the impact parameter vector) in heavy ion collisions. This measurement, though nearer to the central arm rapidity, provides a very useful high resolution addition to the reaction planes determined from the muon piston calorimeter (MPC) and BBC.

Fig.14 shows the correlation between the collision vertex location reconstructed using BBC and VTX data; an excellent correlation is visible. The right panel shows the reconstructed beam spot size transverse to the beam direction. The ability to reconstruct the beam spot with high resolution represents a new capability for PHENIX.

Internal alignment of the VTX detector was performed using tracks from the Run-11 data, achieving a few tens of microns precision. In addition, the VTX was aligned with the other PHENIX detectors; this alignment is maintained after movement of the central arms
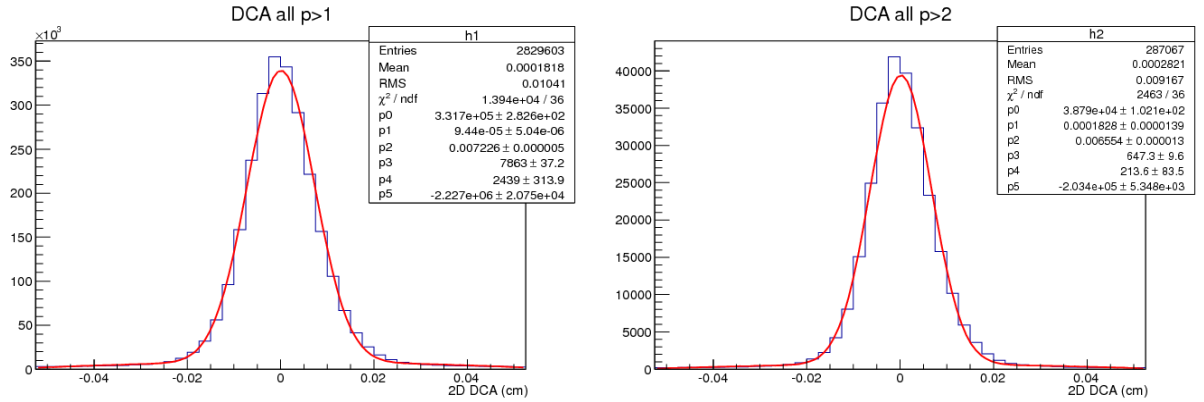
Figure 15: (Left) DCA resolution from Run-11 data for particles with $P_T > 1GeV$. (Right) DCA resolution from Run-11 data for particles with $P_T > 2GeV$.

using zero field data. The alignment achieved is sufficient for charm/beauty separation, since the expected distance-of-closest-approach (DCA) resolution with perfect alignment ranges from 50 to 100 microns, depending on particle transverse momentum. Fig. 15 shows DCA distributions obtained from Run-11 data for different particle momenta. At high transverse momentum (>2 GeV/c) the DCA resolution is 65μm.

Software tools were developed for embedding simulated single tracks into real data events to quantify the tracking and DCA reconstruction efficiency in high multiplicity environment. Figure 16 shows the DCA distribution for electrons from B meson decays predicted by PYTHIA, and the reconstructed DCA distribution for the same electrons embedded in 0-20% most central Au+Au events from Run-11. As one can see, the shape of DCA distribution is almost unchanged after reconstruction up to $DCA = 5mm$. This is sufficient for charm/beauty separation. Reconstruction and analysis of the Run-11 data set is underway.

4.3 Muon Trigger (MuTrig)

The *W*-program in PHENIX is heavily dependent on the upgrades of the muon system in order to efficiently identify high momentum muons and trigger on them. This system has two principal components which were commissioned before and during 2012. Additional trigger cards for the front-end electronics of the muon tracking chambers (MuTr)
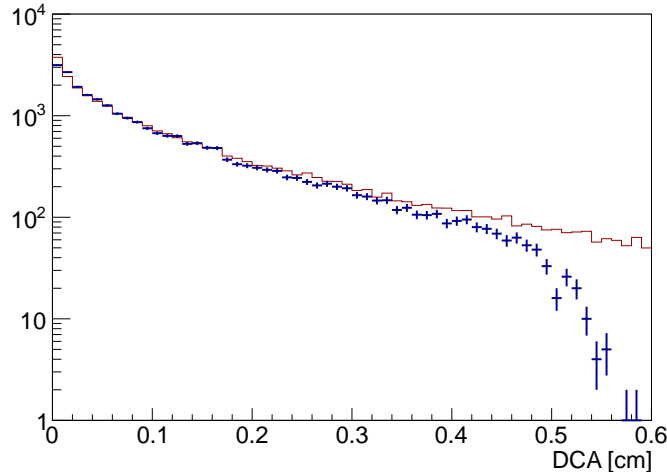
Figure 16: DCA distribution for electrons from B meson decays predicted by PYTHIA (red), and the reconstructed DCA distribution for the same electrons embedded in 0-20% central Au+Au events from Run-11 (blue). The red histogram was re-normalized to show that the shape of reconstructed distribution is almost unchanged.

provide the necessary capabilities to include the muon tracker information in the trigger chain (funded by the Physical Society of Japan). Resistive plate chambers (RPC) in front of (RPC1) and behind (RPC3) the existing muon arm detectors combine additional track information with good timing resolution for the trigger system (funded by the U.S. National Science Foundation). The MuTr front-end boards send data via optical fibers to new transition boards where the signals are reformatted for each of the muon spectrometer octants. The octant based signals are bundled with RPC signal and are then sent to FPGA trigger processor boards (local level-1, LL1).

The trigger decisions in the LL1 are based on a matching of the high momentum MuTr tracks with hits in the RPCs. The timing from the RPCs is further used to reject beam backgrounds in the trigger decision and to connect the recorded event to the correct bunch crossing and, therefore, the correct beam polarization. The RPC3 system was installed and commissioned for Run-11. RPC1 was added during the shutdown in the summer of 2011 and commissioned in Run-12. All detectors were ready for data taking during the 510 GeV p+p run in 2012 (i.e. for Run-12 W Run). RPC3 was in the LL1 trigger for regular operations in Run-12. We note that RPC1 is required at the trigger level mainly for the highest luminosities. The RPC1 system integration into the trigger scheme was completed during the U+U part of Run-12 and is ready to go for high luminosity operations in Run-
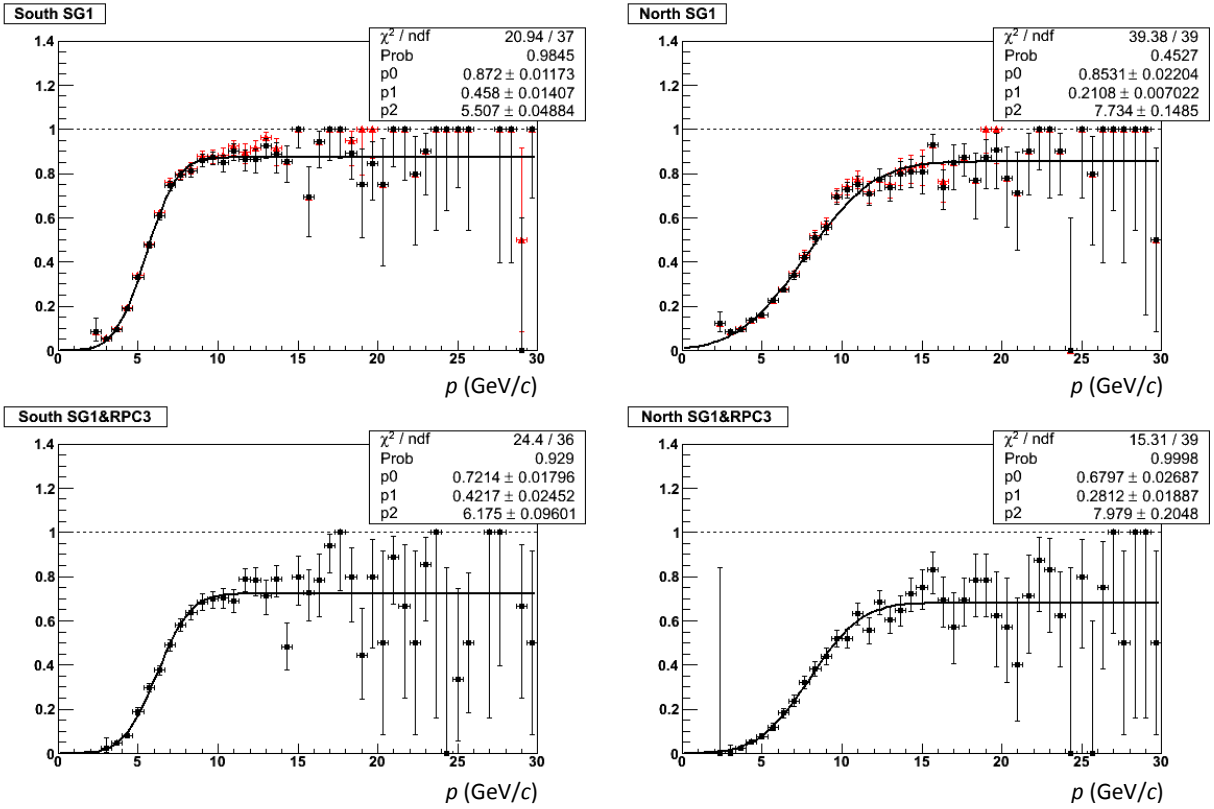
Figure 17: Muon trigger efficiency during the Run-12. The top shows the efficiencies of South (left) and North (right) of the SG1 trigger with the MuTrig FEE upgrade (compared to emulations in red). The bottom plots include the RPC3s in the trigger selection.

13.

Two stainless steel absorbers were added up-stream of RPC1 to further reduce the low-momentum hadron contribution behind the central magnet yoke; these hadrons can decay leptonically and cause fake high-p_T tracks in the muon system. Also, a set of concrete absorbers had to be added in the tunnel area in order to shield the otherwise exposed RPC3 system from beam backgrounds caused by scattering from various dipole magnets up-stream of the PHENIX-IR.

Figure 17 shows the efficiencies of the high p_T trigger on the smallest track sagittas (SG1) with the new MuTrig FEE upgrade in operation. Differences in the turn on are due to the geometrical acceptance and may vary depending on the noise in the respective octants.
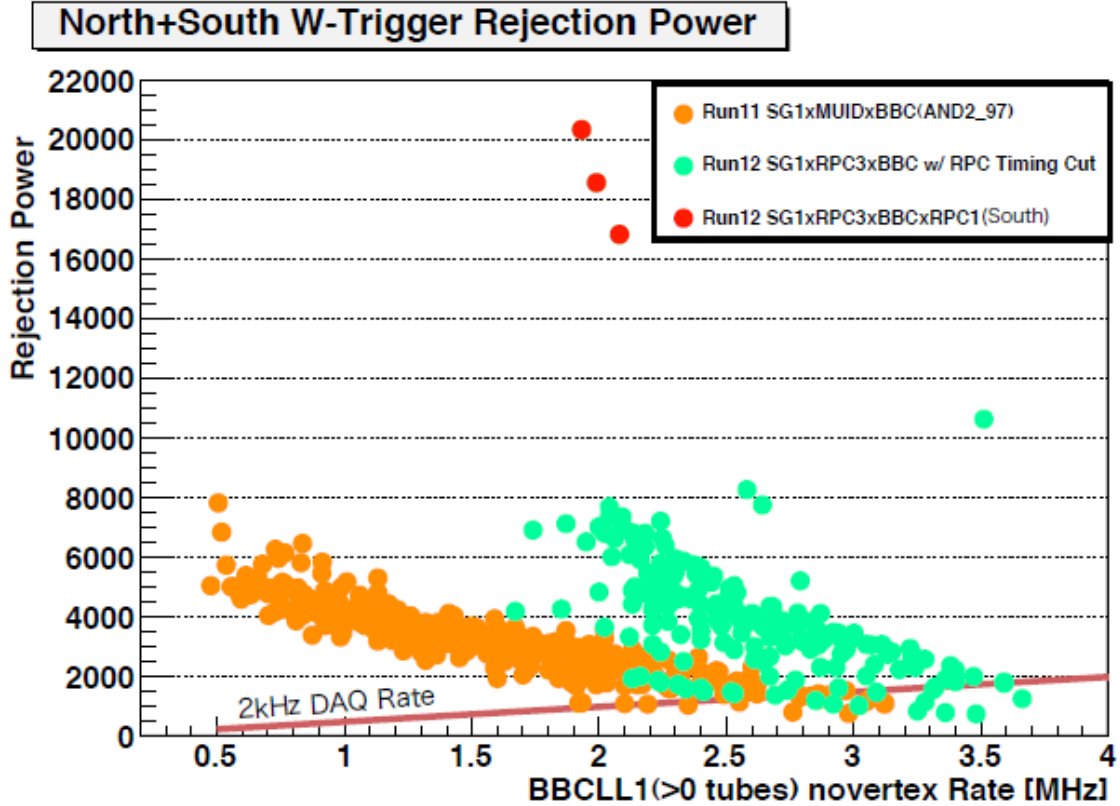
Figure 18: Muon trigger rejection rate during the Run-12 with the new electronics and RPC3 compared to previous Runs. The red line represents the requirement for the trigger to record the full luminosity of the desired *W* production based on the dedicated data acquisition bandwidth.

The turn on of the trigger is well described in simulations and the efficiency reaches a saturation of around 85% at momenta above 10 GeV/c.

Figure 18 summarizes the rejection power of the newly commissioned trigger with data from the RPC3 octants. The red line shows the required rejection power of the SG1 trigger to record all high-p_T muons, as a function of the BBC raw rate At the highest BBC rates, above 3 MHz, it is obvious that the current configuration needs additional improvement. This will be obtained by replacing the BBC with the RPC1 in the trigger. This scheme was tested in Run-12 and was shown to provide an additional factor of 2-3 rejection. As visible by comparing the dots and red line in Fig. 18, this is sufficient.

During data taking in 2011 and 2012, the performance of the new systems was monitored in parallel with all other systems. At the same time we performed fast-track offline analysis to get rapid feedback on background and efficiencies. The full Run-11 data set has been already been analyzed. The resulting preliminary cross section and parity violating asymmetry have been shown at the spring conferences in 2012.

4.4   Data Acquisition (DAQ)

Over the past several years, we have implemented the DAQ2010 plan. This entailed increasing the data throughput capacity to handle increased Au+Au luminosity, developing a second generation data collection module (DCM II), switching the DAQ network to 10 Gb/s Ethernet to make effective use of the DCM II, and performing R&D on improved triggers. These upgrades allow PHENIX to take data at the same rates after installation of the VTX and FVTX.

Increased data throughput relies on an enhanced system of buffer disks in the PHENIX counting house. Other improvements include multievent buffering in the front end electronics, further development of data compression algorithms, and utilization of the new low-level RF system to minimize switching of the PHENIX master clock.

5   Beam Use Proposal for Run-13 and Run-14

5.1   Assumptions about RHIC and PHENIX performance

The physics performance evaluations in this document reply upon projections for RHIC luminosity and polarization in Run-13 and Run-14, as well as expectations for PHENIX performance efficiency.

For the RHIC expectations, we utilize updated projections from Wolfram Fischer of CA-D. Au+Au projected luminosity was taken from the document posted by CA-D in October 2011. Expected performance for 510 GeV $p+p$ collisions was sent to the experiments on

April 24. The luminosity projection is shown in Fig. 19, and the expected polarization was stated to be between 50 and 60%. Consequently, we assumed a mean polarization of 55%. It is clear that for a conservative luminosity assumption, midway between the projected minimum and maximum, other improvements would be necessary in order to attain the W physics goals in 10 weeks. However, should the actual luminosity approach the maximum projection, this would be feasible.

For this reason, we request a change in the mode of operation compared to Run-12. In 2012, data taking was interrupted weekly for some combination of maintenance, APEX studies and machine development. We note that the return to stable operations following the stoppage on each Wednesday took long enough to impact the total integrated luminosity in a noticeable fashion. Figure 20 shows the daily accumulated luminosity for the 2012 510 p+p Run. It is clear that steady accumulation occurred only ≈3 days each week. While this operation mode was acceptable in 2012 in order to allow development of the 510 p+p capabilities, the end effects would extract a large penalty during the major physics production run requested for 2013. Consequently, we request an operations mode that involves breaks for machine development, APEX studies, and/or maintenance on a two-week rather than one-week cycle.

The luminosity estimates utilized in our performance studies for low energy p+p comparison running were provided to PHENIX by Wolfram Fischer on May 17. We appreciate these projections, as they reflect estimation of performance at rigidities new for RHIC. We understand that the constraints arise from space charge and beam size in the triplets, and that at some of the energies considered it is not possible to establish collisions at both experiments. Nevertheless, we find the comparison running compelling, as detailed below.

The PHENIX performance projections assume the following factors in our data taking efficiency.

- The PHENIX DAQ livetime is 91%.

- The PHENIX up time (i.e. fraction of the time when beams are colliding that the PHENIX DAQ is running) is 75% for ion running and 70% for polarized p+p running.

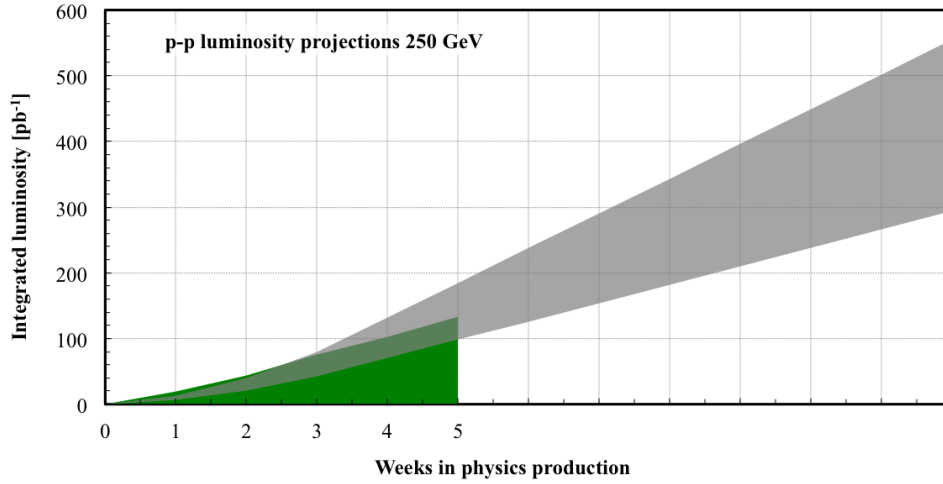- The fraction of collisions inside a ±30 cm vertex cut is 60%, and 30% inside ± 10 cm.

26

Figure 19: Projected 510 GeV $p+p$ luminosity in Run-13.
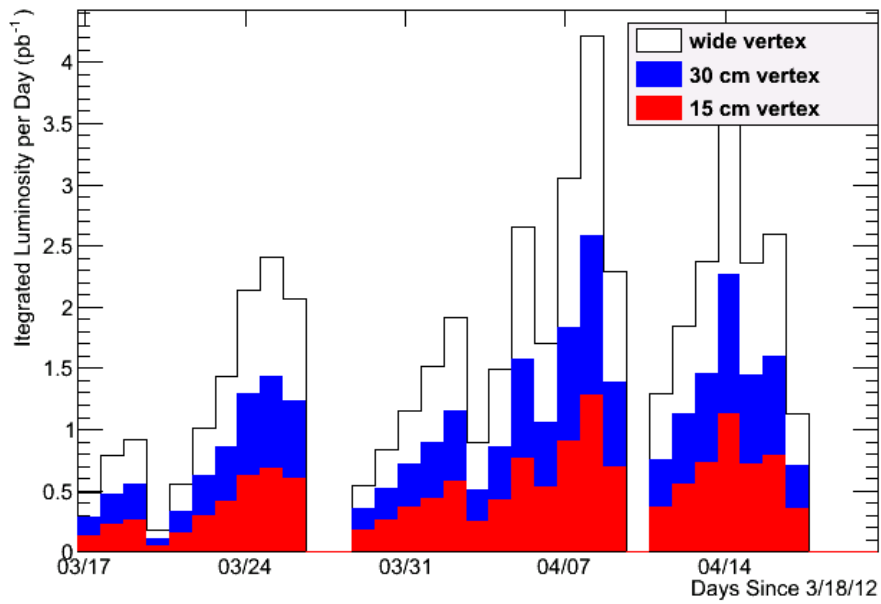

Figure 20: Daily accumulate 510 GeV $p+p$ luminosity in Run-12.

The difference in up time between ion and polarized proton running is due to the need to ramp down high voltages for polarimeter runs to measure the polarization. Our physics performance projections take into account the now well-quantified data taking efficiency penalty of 10% associated with commissioning new detector systems. Of course, this penalty is not included for Runs without commissioning activities.

5.2 Spin Physics Goals for Run-13

The PHENIX spin physics goals in Run-13 and beyond are closely tied to NSAC milestones HP8 and HP12, namely the measurement of the quark and anti-quark helicity distributions through parity violating longitudinal spin asymmetries and the gluon spin contribution to the proton in the range $0.01 < x_g < 0.3$. These measurements are consistent with previous beam use proposals as well as the recently submitted decadal plan for the years 2011-2020 [30].

5.2.1 Machine performance

In the following we present updated projections for a recorded integrated luminosity of 300 pb^{-1} which are based on analysis of data from 2011. These data includes changes in the detector configuration and understanding of signal to background ratios that are of key importance in the extraction of the W-boson single spin asymmetries.

Our projections are based on the latest guidance from the Collider Accelerator Department regarding luminosity and polarization expectations. In Run-12, the center-of-mass energy for the W-boson production has been adjusted from $\sqrt{s} = 500$ GeV to 510 GeV for which an increased polarization lifetime was predicted from simulations. Since any changes in our physics program are minimal between these two energies and our projections are based on 500 GeV, we are using 500/510 GeV interchangeably.

The RHIC performance was extremely successful in Run-12 in terms of luminosity development. There were many very important APEX sessions. In Run-13, RHIC will utilize a new polarized proton source and commission an electron lens, both of which are important for the successful completion of the spin program with high luminosities. We

emphasize that after tune-up and ramp-up, highest operational priority must be given to integrating luminosity for physics.

Our highest priority for Run-13 is the *W*-program. Beam polarizations are expected to be between 50% and 60%, depending primarily on successful commissioning of the new polarized source. Per the CAD guidance, we assume an average polarization of 55% for Run-13 at 510 GeV. The average expected delivered luminosity for a 10-week period of physics collisions is in the range of 350 pb^{-1}. If we fold in the PHENIX data taking efficiency (up-time) and the collision vertex distribution, this will provide the major part of the required luminosity. With a delivered luminosity near the high end of the expectation range, we are within reach of finishing the program at 510 GeV with a few additional weeks of running. As noted above, this will likely require machine operations in a mode that integrates luminosity for physics with biweekly, rather than weekly, breaks for machine development, APEX studies, and maintenance.

5.2.2   Single spin asymmetries in *W*-production

The parity-violating single helicity asymmetry $A_L(W^{\pm})$ of *W*-bosons directly correlates the valence quark and sea anti-quark polarizations in the proton in an experimental observable. PHENIX measures *W*-bosons via their weak leptonic decay $W^{\pm} \rightarrow l^{\pm}\nu$. In order to identify the *W*-decay in electrons/positrons in the PHENIX central arms or muons in the forward muon arms, it is necessary to measure the respective high-p_T leptons.

Figure 21 shows the expected sensitivity of our measurement with a signal-to-background ratio of 1:1 in the forward/backward region ($1.2 < \eta < 2.2$). The reduction of background contributions in high-p_T muons is extremely important in this region where we don't observe a Jacobian peak from the *W*-decay. The projections are based on the analysis of data from Run-11 with comparisons to extensive simulations of punch-through hadrons and muons from other decay channels. The data already includes RPC3 but does not have information from RPC1 yet. Also, we expect an additional reduction of background from tracking in the newly commissioned VTX and FVTX detectors. This will be optimized starting with the Run-12 data.

Our projections are based on a total sampled luminosity of 300 pb^{-1}. This, of course, depends on the vertex distribution which currently contains about 2/3 of the delivered luminosity in a z-range of $|z| < 30$ cm. The assumed signal-to-background ratio can be
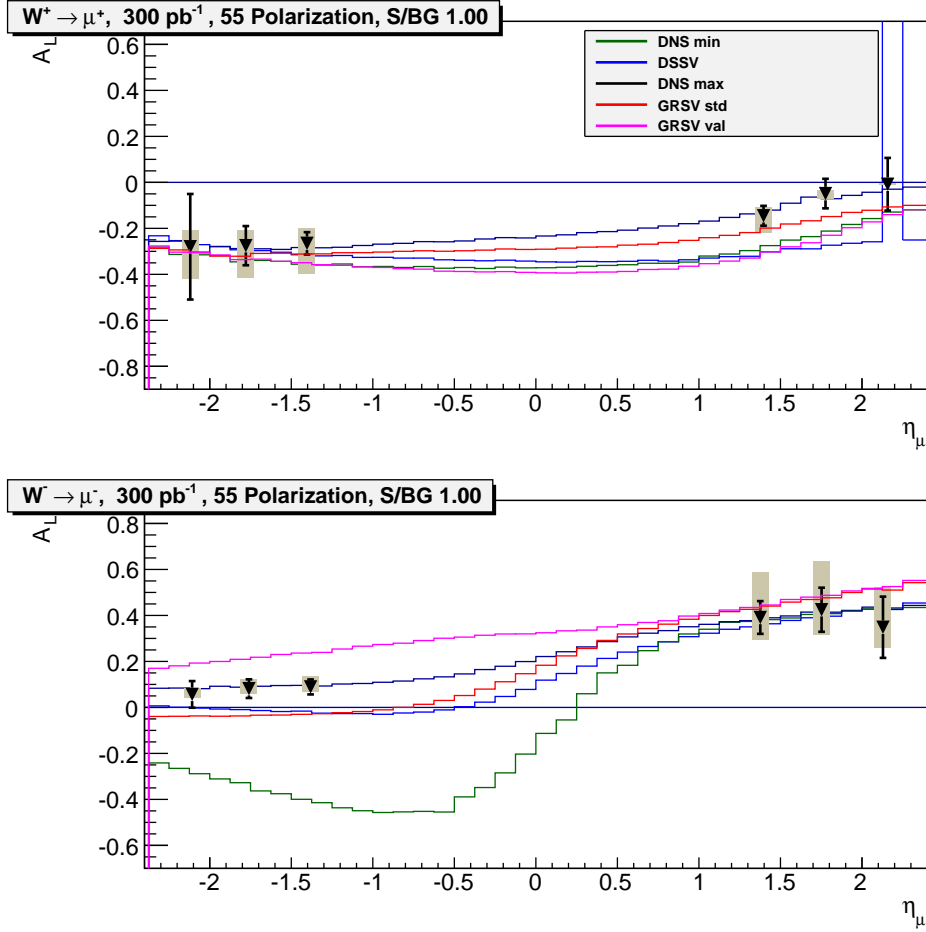
Figure 21: Expected single spin asymmetry of high-p_T muons in $p+p$ collisions at $\sqrt{s} = 500$ GeV with an average beam polarization of $P = 55\%$. Signal to background ratios are assumed to be S:B=1:1 in a sampled integrated luminosity of 300 pb^{-1}.

considered a conservative estimate using the available detectors in Run-13. Naturally, what counts in the end is the figure-of-merit which will be a combination of samples with reduced vertex requirements for better background rejection and increased samples with wider vertex distributions than include more background.

Figure 22 shows the expected asymmetries for electrons/positrons in the central arms. This measurement will be much improved compared to the previous publication [23]. The projection is based on new simulations that include the VTX and FVTX detectors
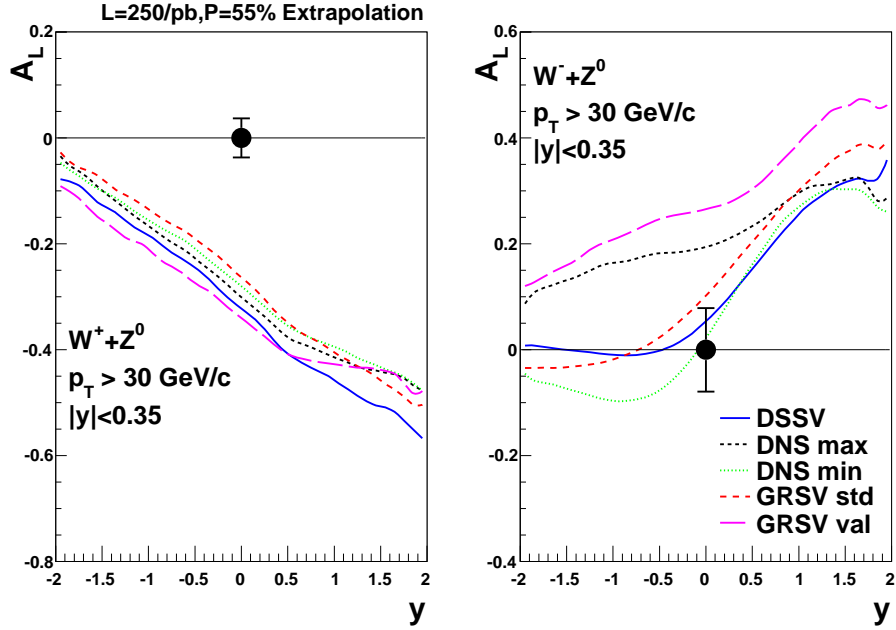
Figure 22: Expected single spin asymmetry of high-p_T electrons/positrons in $p+p$ collisions at $\sqrt{s} = 500$ GeV with an average beam polarization of $P = 55\%$ and a sampled integrated luminosity of 300 pb^{-1}. The signal-to-background fraction is a conservative estimate that does not yet include improvements of the track reconstruction from the VTX.

which introduce about three times more radiation length as the previously installed HBD in the central region of the PHENIX detector (X/X_0=13.3% compared to 3.3% in 2009). The amount of material in this region is critical for the understanding of background contributions in the form of conversion electrons. Charged tracks and photons from π^0-decay remain unaffected and are scaled up according to luminosities compared to 2009 experiences. Figure 22 shows a conservative estimate of the signal-to-background fraction, in which the VTX material is treated as purely dead material. In the future, we expect to reach a signal-to-background fraction that is comparable to the published results with additional information from the VTX detector for the event selection.

5.2.3 Gluon polarization

PHENIX has measured double helicity asymmetries of various probes in the past and has well established techniques for reducing systematic uncertainties due to differences in luminosities. It has previously been shown that measurements at $\sqrt{s} = 500$ GeV will provide access to a lower x-range as compared to existing data at $\sqrt{s} = 200$ GeV. Additionally, PHENIX uses electromagnetic calorimeters in the forward direction (MPC) to extend the x-range further. These calorimeters have been equipped with new electronics during Run-12 to enable a dedicated trigger based on the transverse momentum of clusters. At the same time it can be used to trigger on correlations of two clusters. The trigger threshold is set such that we can sample the full luminosity with a fraction of the total PHENIX bandwidth in parallel to the W-program.

These particle correlations are powerful in that they constrain the x-range of the partons in the hard scattering process more accurately than any simple change of collision energy. We are therefore able to select different x_{gluon} depending on hadron pairs in central-central, central-forward, or forward-forward correlations. Figure 23 shows the expected asymmetries of inclusive clusters and of back-to-back correlations with the MPC. With the MPC we are not limited to a narrow z-vertex region and can use the full delivered luminosity. We estimate that we can sample 200 pb^{-1} for this measurement. (left and middle part of Fig. 23 with the PHENIX efficiency already folded in). For correlations with π^0 in the central arm (right part in Fig. 23) are restricted to a range of ± 30 cm in z which is included in the trigger efficiency for the projections already. Our projections are based on different scenarios of helicity parton distribution functions from the latest DSSV global analysis [31] where DSSV$_{max}$ represents the upper limit of our current knowledge.

5.2.4 Special beam studies

As has been pointed out above, the measurement of, especially, double helicity asymmetries requires a good understanding of several sources of systematic uncertainties. With the expected sampled luminosities the relative luminosity between the different helicity states will become the major contribution on the order of 10^{-4} to the total error in inclusive measurements. From recent special beam studies with transverse polarization in Run-12 we have learned that there can be significant contributions to the different luminosity estimates from remnant transverse asymmetries of neutrons in the ZDC. These
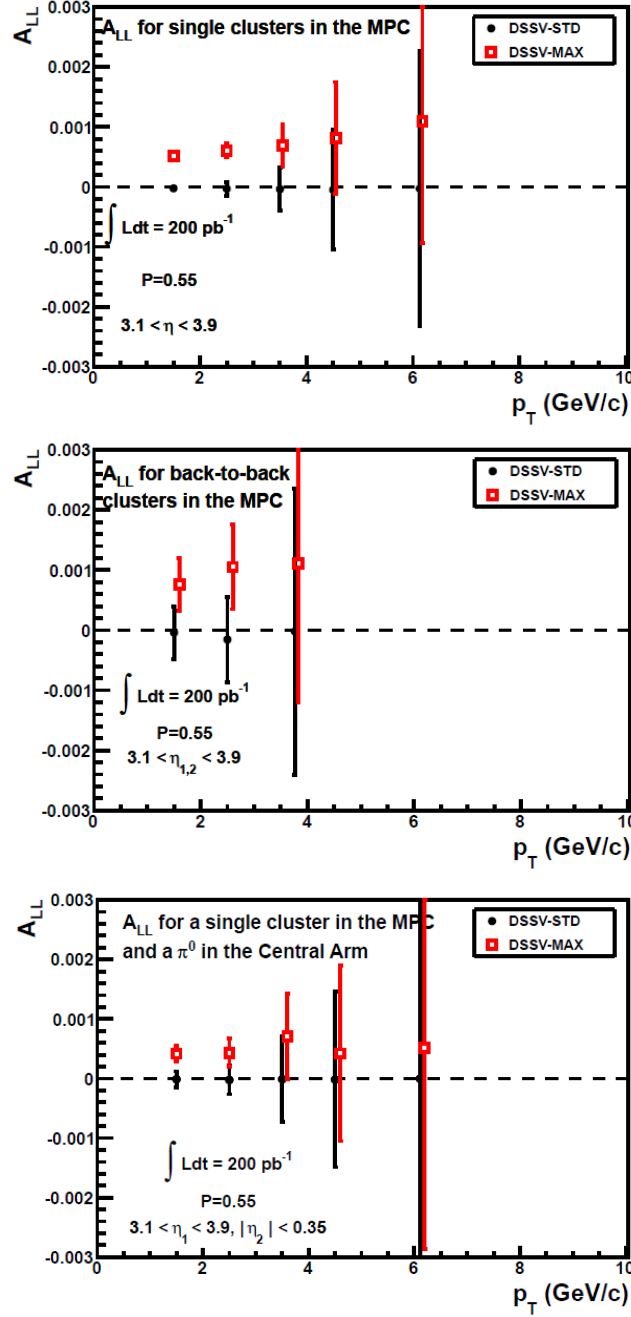
Figure 23: Cluster double helicity asymmetry projections measured in the MPC. Estimations of the asymmetry are based on two different scenarios of parton distribution functions in the DSSV global analysis [31]. (upper) inclusive single cluster asymmetries, (middle and lower panels) back-to-back correlations of diclusters and cluster-π^0, which sample different ranges of the partonic momentum x.

33

studies have been carried out at 200 GeV where $A_N(n)$ has been measured before [10].

It is preferable to do the same studies at 500 GeV in order to directly measure the impact of a transverse polarization component during the longitudinal running. These studies include an extended angle scan and displaced collisions with respect to the nominal collision point. In total we estimate four RHIC fills for this.

Another source of systematic uncertainties stems from the double transverse asymmetry A_{TT}. This asymmetry is expected to be small, but has not been measured so far. Since it scales directly with the transverse polarization squared, we only require a small amount of data comparable to that of the mentioned special beam studies.

In this context, we would like to point out the importance of a small residual transverse component of the polarization which directly scales the impact of A_{TT} on any double helicity measurement. We assume $\Delta P_T/P < 0.05$ in all our projections. PHENIX is able to track this transverse component based on scaler data in near online mode which will provide feedback to CA-D regarding the effective settings of the spin rotators. It is also desirable to tune the currents of the spin rotators surrounding PHENIX and STAR synchronously because they can affect the polarization vector globally in RHIC.

5.2.5 Transverse spin physics

In addition to the helicity measurements at $\sqrt{s} = 500$ GeV PHENIX proposes to take data at 200 GeV with transverse polarization. This request is primarily driven by the need for comparison data for the heavy ion program with the newly commissioned (F)VTX detectors. At the same time, though, the luminosity requirements are in good agreement with the transverse spin physics program. Previously, we have recorded and analyzed about 8 pb^{-1} (runs 2006 and 2008) and recorded an additional 9.2 pb^{-1} in 2012 with beam polarizations of 50% or more.

The proposed transverse running will make it possible to improve the existing measurements with significantly increased statistical precision and extend the transverse momentum range beyond our current knowledge to $p_T = 6$ GeV/c. In particular, this is of interest in the behavior of transverse single spin asymmetries where higher twist descriptions descriptions predict a saturation and turn-over of A_N. Currently this turn-over has not
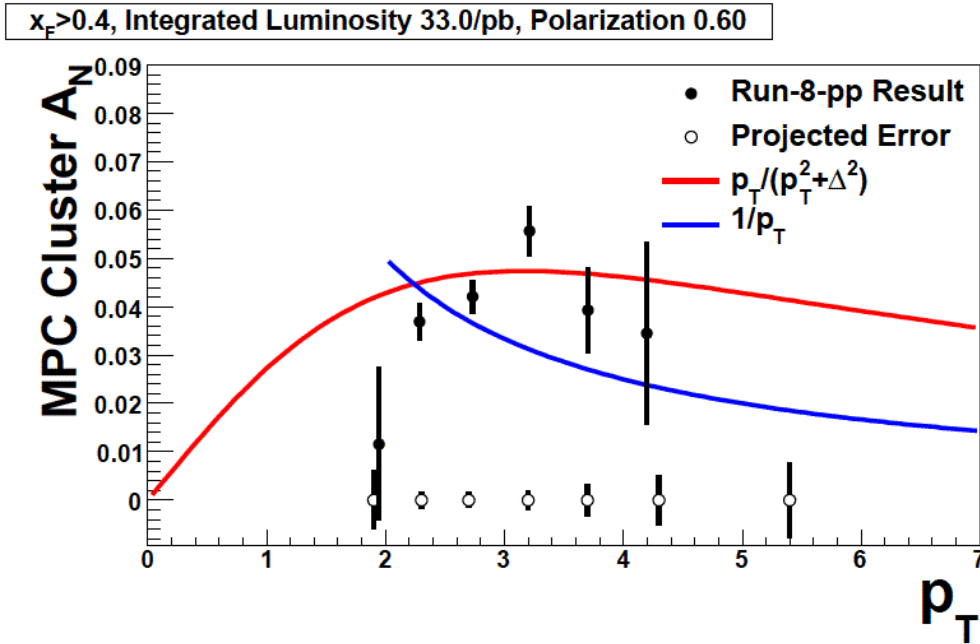
Figure 24: Projections (open circles) for inclusive cluster transverse single spin asymmetries in forward direction. The lines represent the functional form of the expected decrease of the symmetries with growing p_T that has not been observed so far. The solid points are PHENIX preliminary results from the Run-2008.

been observed and it is not yet clear what functional form of p_T the asymmetry follows. Figure 24 shows the expected statistical accuracy of electromagnetic clusters as measured in the MPC in a data set of 33 pb^{-1} total integrated luminosity.

It is generally recognized that transverse single spin asymmetries in $p+p$ collisions can arise from different mechanisms in the initial and final state. In the initial state, a correlation of the parton's k_T dependence with the spin direction of the proton will create such an asymmetry (Sivers effect). Also, a spin dependent fragmentation in combination with a transverse quark polarization can lead to the same result (Collins effect and transversity). Both have been observed in semi-inclusive deep inelastic scattering, but it is so far not clear how they contribute to the observed asymmetries in hadronic collisions.

Figures 25 and 26 show our expectations of two observables that will help disentangle the different effects in $p+p$ collisions, namely a so-called interference fragmentation function and a correlation in two back-to-back hadrons. The interference fragmentation function
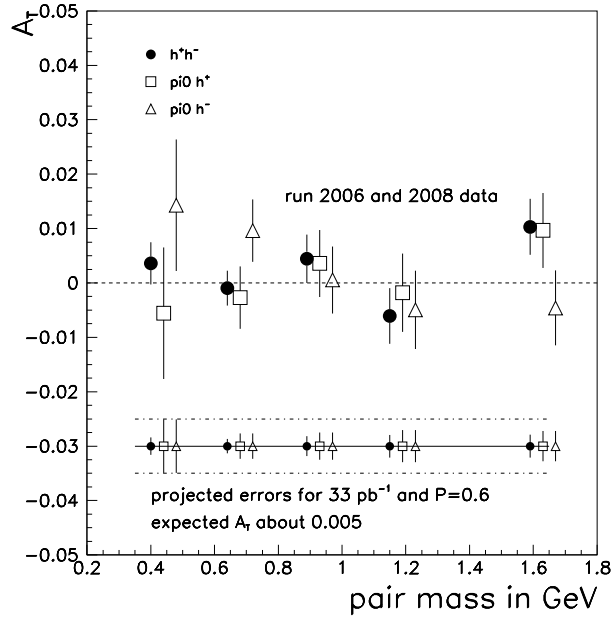
Figure 25: Preliminary results of interference fragmentation functions in PHENIX from Runs 2006 and 2008 are shown with projections for a sampled luminosity of 33 pb^{-1}. Shown are three different combinations of hadron pairs for the central arms.

relates the transversity of the quarks with the Collins fragmentation of two hadrons which is universal and has been measured separately in $e^+ - e^-$ annihilation [40]. The asymmetry in back-to-back correlations of two hadrons probe the Sivers effect in terms of a transverse momentum of partons in the initial state.

Open heavy flavor production is dominated by gluon gluon fusion at RHIC energies. Since the gluon exhibits no transversity, the Collins contribution to any measured transverse single spin asymmetry is fully suppressed. Transverse A_N of open charm is there-
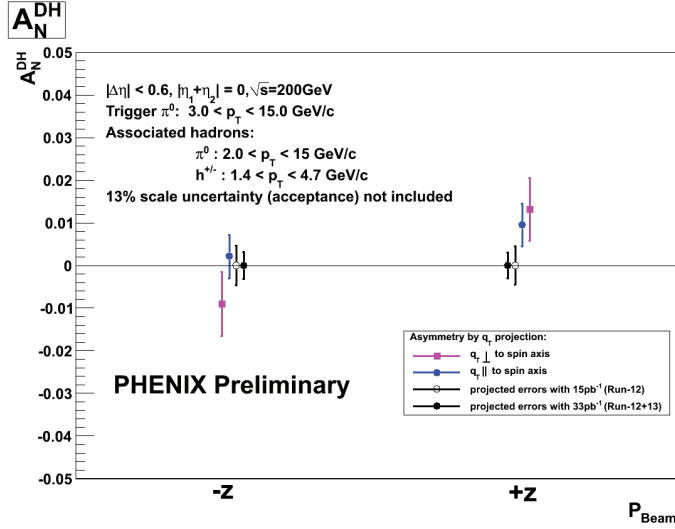
Figure 26: Projected uncertainties for back-to-back two hadron correlations at $\sqrt{s} = 200$ GeV based on previous preliminary results measured with the PHENIX central arm detectors.

fore directly sensitive to the gluon Sivers function. At the same time it has been shown that it is sensitive to trigluon correlation functions in the collinear, higher twist approach [34]. The FVTX, in conjunction with the muon arms, will improve the measurement of single muons from c and b decays. Figure 27 shows our projected sensitivity single muon transverse single spin asymmetries at $\sqrt{s}$=200 GeV for an integrated luminosity of 5.5 pb^{-1}.

5.2.6 Drell-Yan feasibility studies

In parallel to the *W*-program at PHENIX, a long run with $p+p$ collisions at $\sqrt{s} = 500$ GeV will provide the first measurement of polarized Drell-Yan production at forward rapidity in the world. With the use of the newly commissioned FVTX detector, cuts on DCA distributions will provide rejection capability for open heavy flavor contributions in the intermediate invariant mass distribution between 4 GeV$/c^2$ < $m_{\mu\mu}$ < 8 GeV$/c^2$ of muon pairs. We assume to collect 1000 well-tracked Drell-Yan pairs per detector arm $(1.2 < |\eta| < 2.2)$ within a *z*-vertex range of ± 10 cm from a sampled integrated luminosity of 50 pb^{-1}.
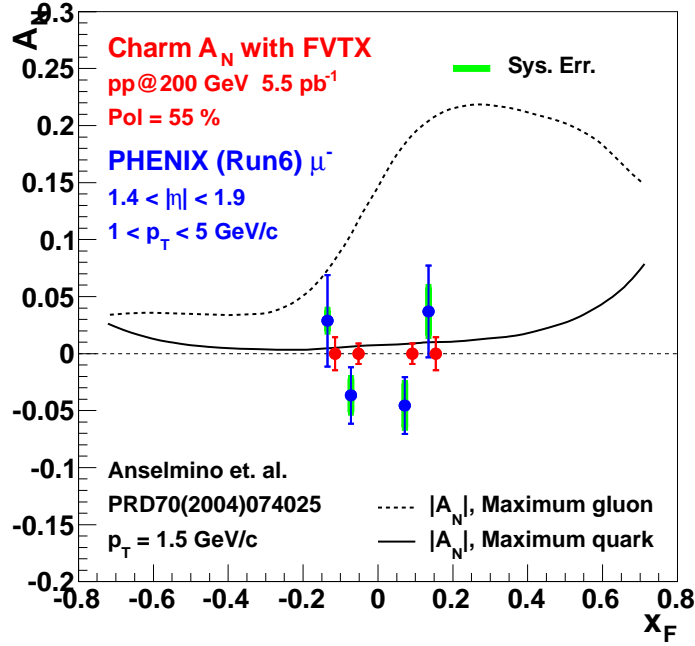
Figure 27: Projections for charm transverse single spin asymmetries with FVTX for an integrated luminosity of 5.5 pb^{-1} within 10 cm z-vertex range. The lines represent the theoretical prediction from [24]. The blue solid points are PHENIX preliminary results from the Run-2006.

This data set will allow us to determine the Drell-Yan cross section with transverse momenta $p_T < 4\,\text{GeV}/c$ as shown in Fig. 28. Results will be comparable to measurements at other energies and, more importantly, to predictions from QCD which will provide helpful input for the determination of the intrinsic transverse momentum k_T of partons in the initial state. The longitudinally polarized data set, with limited statistical accuracy at this time, can also be used for:

- a double-spin asymmetry A_{LL}, which provides a clean access to anti-quark polarization independent of the quark fragmentation process and

- a single-spin asymmetry $A_{LU}^{\sin(2\phi)}$, which provides access to the quark *longitudinal transversity* $h_{1L}^{\perp}$ [41] distribution, a leading order transverse momentum dependent quark distribution which describes the probability of finding a transversely polarized quark inside a longitudinally polarized nucleon.
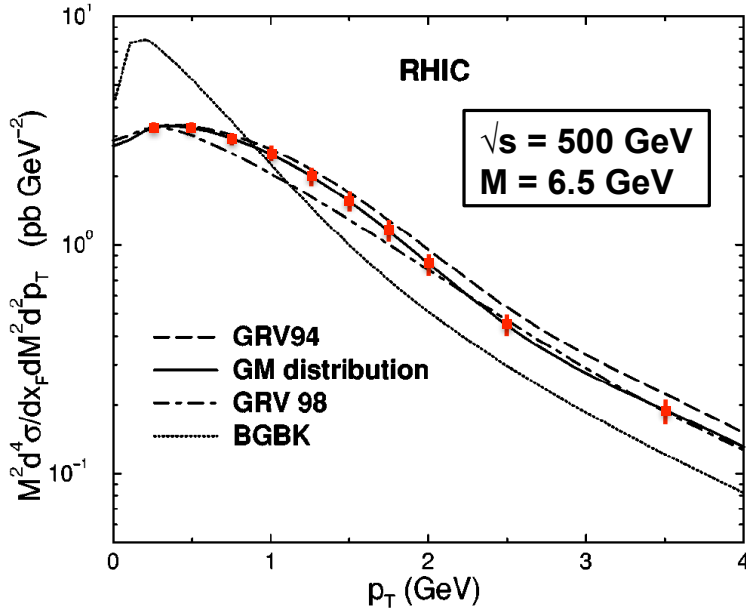
38

Figure 28: The Drell-Yan dilepton transverse momentum p_T distribution. The solid lines are the GM results including unitarity effects; the long-dashed lines are the curves using GRV94 for the gluon distribution (without unitarity effects) in the dipole cross section. The dot-dashed curves are the results obtained with the GRV98 gluon distribution (without unitarity effects) in the dipole cross section and the dotted lines are the results using the BGBK model [26]. Expected PHENIX statistical uncertainties in Run-13 with 50 pb^{-1} recorded luminosity within a vertex cut of ± 10 cm are also plotted as red lines.

5.2.7 Summary

Our highest priority for the Run-13 is completion of the W-program with parity violating single spin asymmetries at 510 GeV. This notion is based on the current detector setup and milestones for the nuclear physics programs in the US and in Japan. Based on the original plans and experiences in the past Runs we expect to collect a majority of the total integrated luminosity within 10 weeks of physics collisions:

Currently, PHENIX has 47 pb^{-1} recorded on tape. Using the latest machine projections from CA-D we estimate about 350 pb^{-1} delivered in 10 weeks with no vertex cut. Assuming that we can increase the PHENIX up-time and make use of a mix of events with a wider vertex distribution we expect to collect the major part of the required integrated luminosity. It is important to note that any variation in the sampled vertex range will require an average signal-to-background ratio of 1:1 or better. Depending on the machine

performance, an additional five weeks will likely enable us to complete the program.

The second highest priority in the spin physics program is on $p + p$ collisions at $\sqrt{s} = 200$ GeV with transverse polarization. Measurement of cluster A_N with the MPC and dihadron A_N and IFF in the central arm require sampling at least 16 pb^{-1} in ± 30 cm. We estimate that four or, or even better, five weeks of data taking on top of the 2012 data will provide the necessary integrated luminosity to reach the projected performance.

5.3   Heavy-Ion Physics Goals for Run-14

There are many measurements of hard probes of the quark-gluon plasma that suffer from limited statistics in PHENIX to date. We have started to combine data from different Runs to improve the precision of such measurements, so additional data taking with 200 GeV Au+Au is extremely useful. The improved luminosity from the full stochastic cooling upgrade makes these measurements more compelling than ever. However, the primary driver for our Au+Au request in Run-14 is heavy flavor physics with the new silicon vertex detectors.

PHENIX has exceptional electron identification in the high multiplicity environment of central Au+Au reactions. This allowed us to make high quality measurements of non-photonic electrons produced by semileptonic decays of D and B mesons. These data showed that there is a dramatic change in the momentum distribution of heavy quarks in the medium. Suppression in Au+Au collisions indicates significant energy loss of heavy quarks in the plasma, while substantially nonzero values of the elliptic flow, v_2, show that the medium effect is sufficiently strong that heavy quarks are caught up and flow along with the bulk. Recently, we have measured heavy flavor suppression at forward rapidity [14] using the PHENIX muon arms.

These heavy flavor suppression continues to present a challenge for perturbative, i.e. weakly coupled, descriptions of partonic energy loss. Strong coupling theories such as those employing the AdS/CFT correspondence, on the other hand, can reproduce the observed behavior. A fundamental complication to quantitative understanding is that the nonphotonic electrons and muons have contributions from both D meson (i.e. charm) and B meson (i.e. bottom) decays. It is expected that D mesons dominate the electron contribution for $p_T < 5$ GeV/c and B mesons for $p_T > 5$ GeV/c. This is roughly confirmed by

examining nonphotonic electron-hadron angular correlations in $p+p$ reactions[17]. However the spectra of D and, especially, B mesons are not yet well known for $p_T > 4\,\mathrm{GeV}/c$ at RHIC.

Diffusion calculations show that bottom quarks are so heavy that they are difficult to move around, and thus should exhibit minimal flow. In the perturbative energy loss framework, radiative energy loss of heavy quarks via gluon bremsstrahlung is suppressed due to the mass dependent "dead cone" effect, where forward radiation for heavy quarks, traveling at velocities much less than the speed of light, is limited. If, contrary to expectations, the bottom quarks exhibit strong flow in the medium, this will challenge the paradigm of perturbative energy loss as a viable way to understand jet quenching. There continue to be debates about the effects and very nature of collisional energy loss of heavy quarks traversing quark-gluon plasma. Precision data are needed to provide constraints, and may be one of the best ways to experimentally probe the existence and nature of quasiparticles for the quarks to collide with.

Furthermore, a measurement of charm flow (separated from bottom flow) out to higher p_T may well provide one of the best constraints on the $\eta/$s ratio via the diffusion approach. This method for constraining $\eta/$s is an excellent alternative to comparing the bulk flow of light hadrons to viscous hydrodynamic models.

Because the two vertex detectors together cover rapidity up to 2.2, PHENIX can study the rapidity dependence of heavy flavor. Collecting an identified open heavy flavor data set for $p+p$, $d+$Au and Au+Au that covers a broad rapidity range will address several key questions. Measuring the rapidity, centrality, and p_T dependence of open heavy flavor modification in cold nuclear matter using $d+$Au collisions will pin down the gluon modification as a function of nuclear density. Open heavy flavor has the advantage over J/ψ that it is not subject to modification by collisions with nucleons, thereby avoiding the complication that arises for J/ψ production, where a breakup cross section must also be determined from the data. There is little theoretical guidance on possible rapidity dependence of the J/ψ breakup

Once the role of cold nuclear matter effects is quantified, the contributions to Au+Au collisions can be predicted, allowing effects of hot nuclear matter on open c and b to be isolated. This will permit the study of energy loss of heavy quarks in hot nuclear matter over a broad rapidity range.

In addition, the FVTX will make important improvements in the quarkonium measurement capabilities at forward and backward rapidities by improving the mass resolution and signal to background ratios for quarkonium measurements. This is particularly important for studying $\psi\prime$ cold and hot nuclear matter effects.

5.3.1 Midrapidity Heavy Flavor R_{AA}, and v_2 with the VTX

One of the most interesting physics topics that became possible when the VTX detector was installed for Run-11 is D and B meson separation at midrapidity. Using displaced vertex information from the VTX, matched to electrons identified in the PHENIX central arms, allows separately measuring D and B meson contributions to the measured electron R_{AA} and v_2. These data will definitively show the fate of charm and bottom quarks in the quark-gluon plasma.

The distance of closest approach, or DCA, distributions from the Run-11 data already indicate this new capability. We have demonstrated successful track matching and the ability to separate decay from prompt electrons. Fitting the measured DCA distributions in different bins of electron p_T allows construction of separate spectra of electrons from D meson decays and those from B mesons.

The quality of the anticipated Run-13 $p+p$ and Run-14 Au+Au VTX data will be improved by replacing a number of ladders with broken wire bonds; ladder repair is currently underway. Coupling this with stable running conditions coming from experience with the detector, and improved statistics, we can expect a much better measurement than the initial one using Run-11 200 GeV Au+Au and Run-12 200 GeV $p+p$ collisions.

By combining multiple runs, including Run-14, we expect to reach an integrated yield of approximately 4 nb^{-1}, corresponding to approximately 29 billion recorded Au+Au interactions with collision vertex inside 10 cm. The requested Au+Au running in 2014 represents approximately one quarter of this full statistics. The VTX, of course, already has an initial data set from Run-12. For comparison $p+p$ measurements at 200 GeV, we project an integrated luminosity over several years of $15\,\mathrm{pb}^{-1}$ sampled within the same z-vertex acceptance. We show the projected physics performance expected for R_{AA} using the entire data set in Figure 29. Expectations from Run-14 alone can be evaluated by doubling the statistical errors.
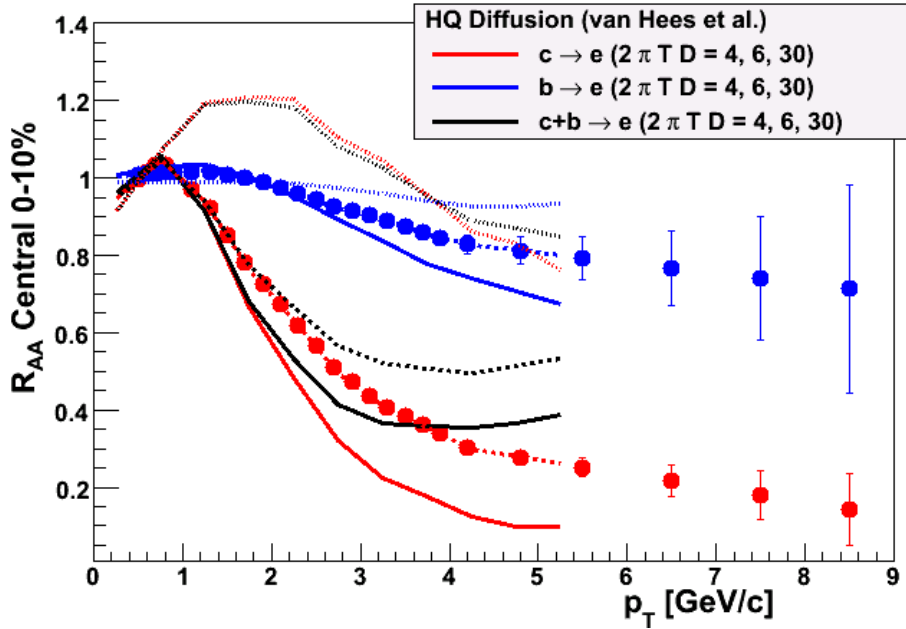
Figure 29: Projected uncertainties for the nuclear modification factor (R_{AA}) as a function of transverse momentum for heavy flavor electrons tagged with a displaced vertex from D meson decay (red) and B meson decay (blue). The uncertainties are for the 10% most central Au+Au collisions—a subset of a total of 29 billion Au+Au minimum bias events and 14.8 pb^{-1} $p+p$ events at 200 GeV. Also shown are calculations by van Hees *et al.* [38] assuming different diffusion coefficients.

Shown in Figure 29 are the nuclear modification factors R_{AA} of electrons from D and B decays. As the first VTX data are currently being analyzed and its performance quantified, these projections assume an ideal detector response and efficiency. Nevertheless, it is clear that the R_{AA} can be well separated to high p_T where B decays should dominate. Figure 29 illustrates that the energy loss of charm and bottom quarks can be separately determined with good precision.

Figure 30 shows the projected uncertainties for minimum bias Au+Au collisions for the elliptic flow v_2 observables. For the elliptic flow projections, we have assumed a reaction plane resolution comparable to that from the reaction plane detector that was installed prior to 2007. This detector was removed after the 2010 running period due to conflicting space requirements with the VTX. However, we have already demonstrated that the VTX can be similarly utilized with good resolution. We anticipate using a reaction plane measured in the FVTX, as well. A reaction plane resolution of 0.75 was achieved with
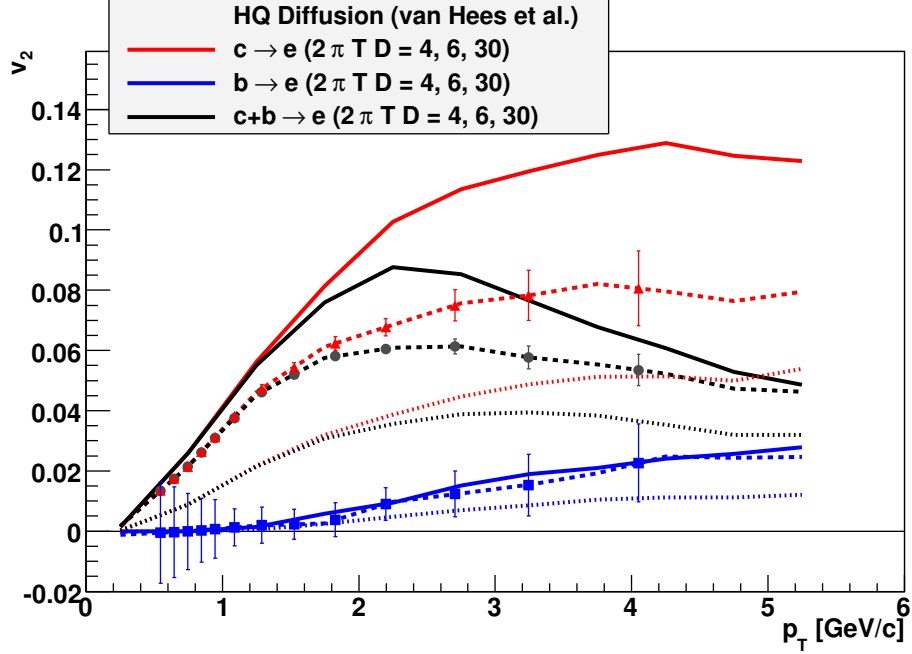
Figure 30: Projected uncertainties for elliptic flow (v_2) as a function of transverse momentum for heavy flavor electrons tagged with a displaced vertex from D meson decay (red) and B meson decay (blue) and the combination of the two (black). The uncertainties correspond to 29.0 billion Au+Au minimum bias events. Lines show calculations from van Hees *et al.* [38] in a heavy quark diffusion calculations assuming different diffusion coefficients. Note that the largest flow magnitude case corresponds to shear viscosity to entropy ratio near the minimum bound.

the dedicated reaction-plane detector in 2007. In Run-14, we anticipate a resolution better than 0.6 using the outer edge of the VTX detector (i.e. the largest rapidity covered) and the entire FVTX detector.

5.3.2 Forward rapidity D, B, R_{AA} with FVTX

The FVTX, in conjunction with the muon arms, will allow clean measurement of single muons from D and B meson decays. This is done by matching reconstructed muon tracks with FVTX information and projecting back to the collision vertex location. The high resolution space points in front of the hadron absorber also serve to remove smearing from multiple scattering in the absorber, thus improving the mass resolution for dimuons. The

expected error bars for forward heavy flavor R_{AA} are shown in Figure 31 for $\sqrt{s_{NN}}$=200 GeV Au+Au integrated luminosity of 0.8 nb^{-1} and using as reference 5.5 pb^{-1} of 200 GeV p+p data. These correspond to the request for Run-14.

The heavy flavor R_{AA} at forward rapidity projection is based on a full muon-arm and FVTX simulation which takes into account all reconstruction efficiencies and analysis cuts that are needed to pull the heavy-flavor signal out from the hadronic backgrounds.

We have also included trigger efficiencies in our projections. In central Au+Au collisions, large background rates make triggering on single muons very difficult. However, we will continue to record a very large fraction of the min-bias events with a collision vertex inside the VTX acceptance (i.e in $\pm$ 10cm). Judging from Run-11 and Run-12 performance of RHIC with stochastic cooling, we estimate that we will record approximately 80% of all collisions with vertex inside $\pm$ 10 cm. Consequently, the Run-14 FVTX projections use 0.8 nb^{-1} for the Au+Au integrated luminosity. For p+p data taking we expect to collect around 30% of single muons, using the PHENIX standard Muon Identifier one-deep trigger, which will provide sufficient statistics for R_{AA} measurements in the range of muon $p_T < 3$ GeV. For $p_T > 3$ GeV, we will use a newly developed single muon trigger (SG3) to enhance the high p_T spectrum above the MuID one deep triggered sample. The SG3 single-muon trigger has been implemented in the 2012 200 GeV and 500 GeV p+p running and was found to have an offline efficiency over 70% for both arms. To take these p+p trigger conditions into account in our R_{AA} calculations, we apply a 30% trigger efficiency for $p_T < 3$ GeV and a 70% trigger efficiency for $p_T > 3$ GeV.

We will separate muons from c and b decays by measuring the distance of closest approach (DCA) of the muon tracks with the FVTX detector. The analysis approach is very similar to that described for the VTX, namely an iterative fitting approach is used. The measured DCA distribution in each muon p_T bin is fitted with a sum of distributions from D and B mesons, along with prompt muons and background. The software has been studied extensively and tuned in Monte Carlo. First data from Run-12 are now being analyzed.

The will provide rapidity reach, and complement the studies using the VTX. However, the FVTX data has resolving power of its own to differentiate among different energy loss mechanisms. As seen in Figure 31, already the first R_{AA} measurement of heavy flavor decay muons can resolve the role of collisional energy loss, as implemented in the opacity expansion calculation by Djordjevic, Gyulassy, Levai and Vitev [32]. It is notable that this measurement relies upon the FVTX only for background rejection.
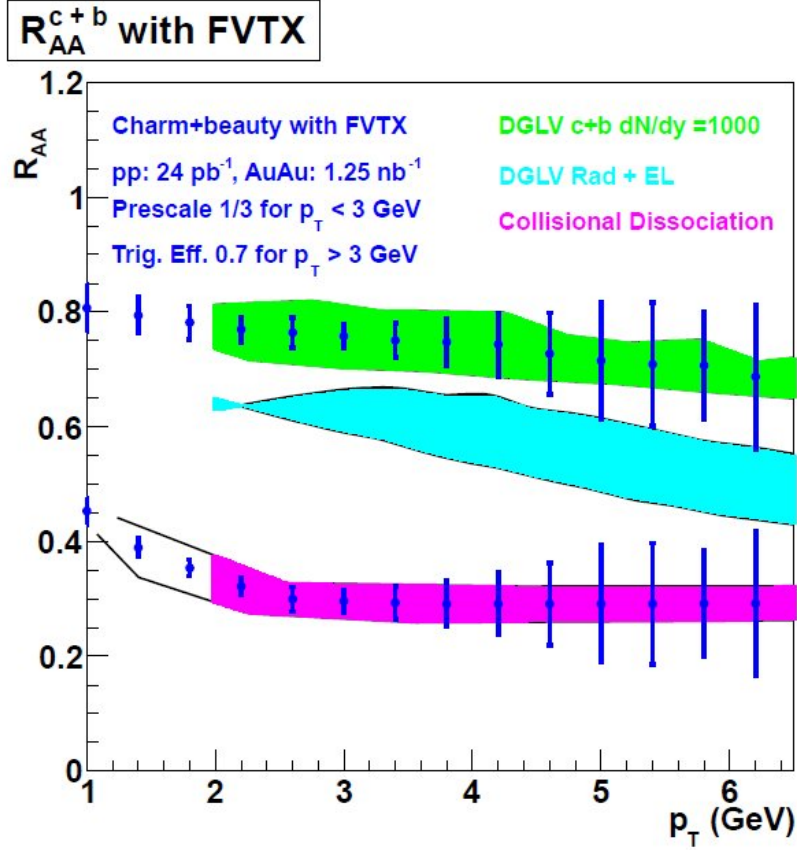
Figure 31: Simulated performance for measurement of R_{AA} of muons from heavy flavor decays at forward rapidity. Fully simulated FVTX detector performance for tagging displaced vertices, along with 0.8 nb^{-1} of 200 GeV Au+Au and 5.5 pb^{-1} of 200 GeV $p+p$ collisions are assumed. Trigger scale down factor of 3 was applied to muon $p_T < 3$ GeV. SG3 trigger efficiency 0.7 is applied to muon $p_T > 3$ GeV.

Different energy loss mechanisms result in different p_T dependencies for charm and beauty energy loss. By using the DCA in the FVTX to separate muons from D and B meson decays, as described above, we can compare their R_{AA} as a function of p_T to distinguish among models of the energy loss. Figure 32 and Figure 33 show the projected error bars of two years of running combined, with Au+Au luminosity of 1.25 nb^{-1} and $p+p$ luminosity of 24 pb^{-1} within 10 cm of the center of PHENIX. The left panel shows, again, the DGLV predictions including collisional energy loss. The right panel shows the results from a calculation that includes collisional dissociation of heavy quark states as they transit the plasma. It is clear the predicted suppressions have quite different magnitudes and p_T dependence, and that PHENIX can discriminate among them.
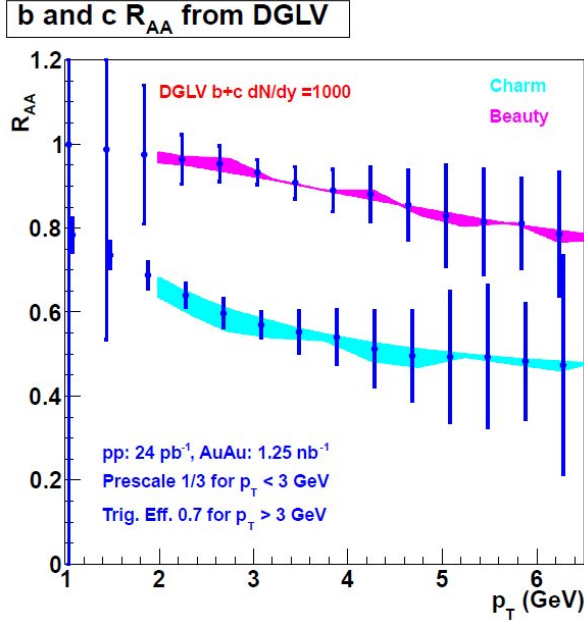
46

Figure 32: Simulated performance for measurement of R_{AA} of muons from b and c decays at forward rapidity with DGLV energy loss model predication. This is for two years of running combined, with integrated luminosities indicated on the figure.
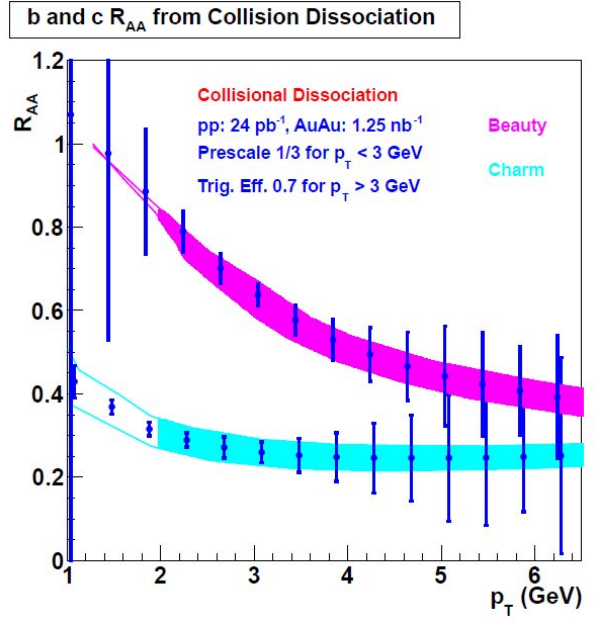

Figure 33: Simulated performance for measurement of R_{AA} of muons from b and c decays at forward rapidity with collisional dissociation energy loss predictions. This is for two years of running combined, with integrated luminosities indicated on the figure

Figure 34 shows the DGLV model [32] b and c energy loss together with the FVTX projection for the requested Run-14 integrated Au+Au luminosity and Run-13 $p+p$ luminosity. Figure 35 shows the same luminosity projection with b and c energy loss from the collisional dissociation model [22]. The statistical error bars are larger, limiting the p_T reach. However, this first measurement will already have significant impact on the theoretical treatment of heavy quark energy loss.

5.3.3 Low energy $p+p$ running for heavy ion reference

Low energy $p+p$ runs are extraordinarily valuable as references to beam energy scan Au+Au measurements. In the 62 GeV π^0 suppression measurement they have proven their usefulness: the physics message altered considerably once we compared the Au+Au
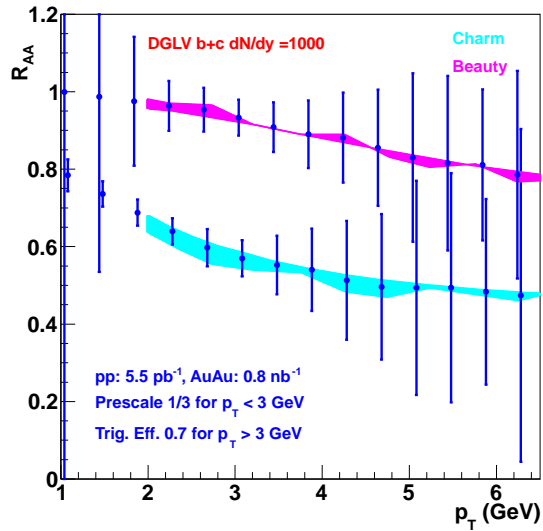
Figure 34: Simulated performance for Run-14 measurement of R_{AA} of muons from b and c decays at forward rapidity with DGLV energy loss model predication.
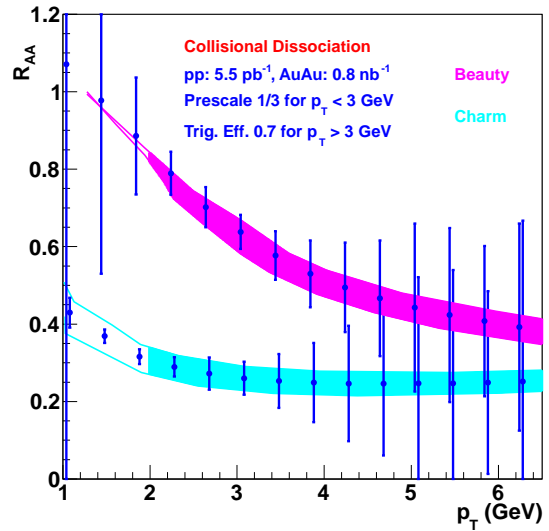
Figure 35: Simulated performance for Run-14 measurement of R_{AA} of muons from b and c decays at forward rapidity with collisional dissociation energy loss model predication.

results to our own measured $p+p$ reference, rather than to the world average of $p+p$ spectra taken at similar energies.

There are two interesting results in the 39 GeV Au+Au data which would be improved by a $p+p$ reference measured in PHENIX. The first is π^0 suppression[13], where R_{AA} has been calculated with external reference (Fermilab E706), measured in a different η range (See the results, Figure 36).

The corrections based on PYTHIA add an error up to 20 % to R_{AA}, in addition to the systematic errors of the Fermilab $p+p$ measurement itself, none of which cancel when applied to RHIC Au+Au data. The other result is J/ψ suppression, where no $p+p$ data exist, so PHENIX measured so far R_{CP} only.

CAD has provided projections for unpolarized 39 GeV $p+p$ collisions. RHIC can deliver approximately $0.6\,\mathrm{pb}^{-1}$ per week. Taking into account the PHENIX efficiencies described above, and a collision vertex cut of $\pm\,30$ cm, we anticipate recording $42\,\mathrm{nb}^{-1}\mathrm{day}^{-1}$.
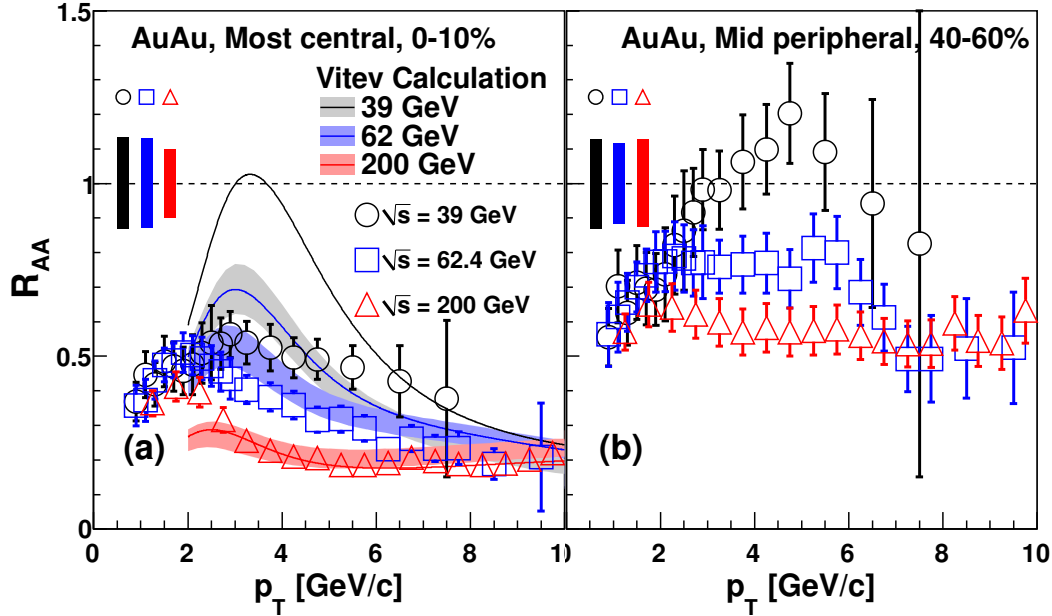
Figure 36: RAA of π^0 in 39, 62 and 200 GeV Au+Au collisions for 0-10 %(left) and 40-60 %(right) centralities. Lines show model calculations from Vitev et al. Note that the $p+p$ reference for 39 GeV R_{AA} calculation is from E706 data with correction of rapidity coverage difference between PHENIX and E706, based on a PYTHIA calculation.

Constructing R_{AA} for J/ψ at 39 GeV would require $0.72 \, pb^{-1}$ $p+p$ reference data, which is about half of the $1.6 \, pb^{-1}$ $p+p$ equivalent to the 30 GeV Au+Au data set. The necessary running time for this is 17 days, i.e. 3 weeks. We judge such a request to be prohibitive in times of curtailed running weeks. However, a 1 week run would yield $0.28 \, pb^{-1}$. Such a sample is sufficient to construct the π^0 R_{AA} up to $\sim$6.5 GeV/c with much smaller errors at 39 GeV. This measurement would address whether R_{AA} decreases significantly at high p_T, approaching the large suppression at higher energies. Therefore, we request 1 week of $p+p$ running at 39 GeV.

5.4 Gluons at low-x in Cold Nuclear Matter using the MPC-EX

Precise knowledge of the gluons in a nucleus would characterize the initial conditions for heavy ion collisions, fixing the initial entropy and fluctuations which lead to the creation of the sQGP. For creation of the bulk hot-dense matter in A+A collisions, the relevant x

is below 10^{-2}. Little is known about the gluon distribution function at $x_{\text{gluon}} < 10^{-2}$ (for the rest of this section x_{gluon} in the heavy nucleus will be referred to as x_2), though there are many attempts to model x_2. Calculations include pQCD extended into the nonperturbative regime, gluon saturation as in the Color Class Condensate (CGC), and parameterizations of modified gluon distribution functions in nuclei, $R_g^A(x, Q^2)$, obtained by fitting deep-inelastic scattering events, Drell Yan pairs, and RHIC midrapidity π^0s. The large uncertainties at low x call for new high precision data that can access low x in nuclei.

d+Au collisions at RHIC include a gold nucleus, but do not make quark-gluon plasma. PHENIX can access the relevant kinematic range to study nuclear gluon distributions by making measurements at forward rapidity. While many processes involve gluons and depend on the gluon distribution, unraveling the nucleon's gluon structure from the data can be complicated. Direct photons, however, are produced in QCD by an inverse Compton process. Scattering of a gluon and a quark results a photon and a quark in the final state. At leading order, this elementary process is straightforward, and the photon travel out of the nucleus unperturbed. Consequently, photons produced in this way offer a promising experimental probe of the gluon distribution function, both through the single photon distributions, and via conditional measurements.

Measuring direct photons is very difficult, as there are large backgrounds of decay photons. At forward rapidity, particles are boosted in the beam direction, and nearby photon pairs from neutral pion or eta decays further complicate the measurement of direct photons. PHENIX has developed a new upgrade, known as the Muon Piston Calorimeter Extension (MPC-EX), to meet this technical challenge and measure direct photons at forward rapidity. The MPC-EX is a Si-W preshower detector in front of the existing PHENIX MPCs. This detector consists of eight layers of Si "minipad" sensors interleaved with tungsten absorber. Detection of the initial shower positions with the high resolution of the silicon and measurement of the shower energy with the high resolution MPC crystals enables identification and reconstruction of π^0 mesons at energies up to ≈ 80 GeV. The MPC and preshower are located at $3.1 < \eta < 3.8$, making them uniquely positioned to measure phenomena related to either low-x partons in the target or high-x partons in the projectile. With the capability of the MPC-EX to reconstruct and reject π^0s (as well as other hadronic sources of photons) at very high energies comes the capability to separate direct photons from other sources of photons.

In order to measure the effect of the nuclear binding upon the gluon distribution, we will use the MPC-EX to measure direct photon production in both $p+p$ and d+Au collisions. While we have planned the measurement using d+Au instead of p+Au for ease of col-

lider operations, recent papers suggest that this could have a deleterious impact upon the sensitivity of the measurement. We are working with the theory community to determine whether this physics is best carried out with d+Au or p+Au collisions, and will provide an update on this question when the 2014 run is discussed by the PAC. In the meanwhile, we have made physics performance projections based upon a full year's d+Au run of 12 weeks. Should it be possible to begin this measurement already in 2014, as we hope, we would certainly begin with d+Au in order to be compatible with the anticipated Au+Au running.

Direct photons from PYTHIA simulations are used to provide distributions and total expected yields in $p+p$ and d+Au collisions. In the figures below, the projected yields assume a total integrated luminosity of 49 pb^{-1} of $\sqrt{200}$ GeV $p+p$, which requires 12 weeks of running and 0.35 pb^{-1} in $\approx$ 12 weeks of $\sqrt{200}$ GeV d+Au. A shorter d+Au run in Run-14 would allow a first look at the physics and help commission the analysis in the multiplicity environment of d+Au collisions.

In our performance studies, direct photon candidates are separated into two η ranges, an inner range of $3.1 < \eta < 3.45$ and an outer range of $3.45 < \eta < 3.8$. The ability of this measurement to constrain parameters in the EPS09 gluon nuclear parton distribution functions is determined by studying how much of the viable region, R_G, is consistent with the data. Results are presented as exclusion plots based upon the measured R_{dAu} and the corresponding EPS09 suppression factors in Figure 37. The central value of EPS09 is taken as the nominal value in Fig.37. However, this is arbitrary as all values in the EPS09 range are equally probable and consistent with the world's data. We vary all systematic errors over three standard deviations in each direction to determine the allowed and excluded region, following standard PHENIX procedure. The hatched area shows the exclusion region at 90% confidence level for all of EPS09 curves, while the light blue band shows the result using the simulated direct photon result from the MPC-EX. The dark blue region represents the MPC-EX exclusion at the 1σ limit. The black lines within the dark blue band are the EPS09 R_G curves that are consistent with the existing fits to world data. It is clear that the proposed direct photon measurement will greatly decrease the band of allowed EPS09 curves, thereby constraining the gluon distribution function in nuclei at small x.
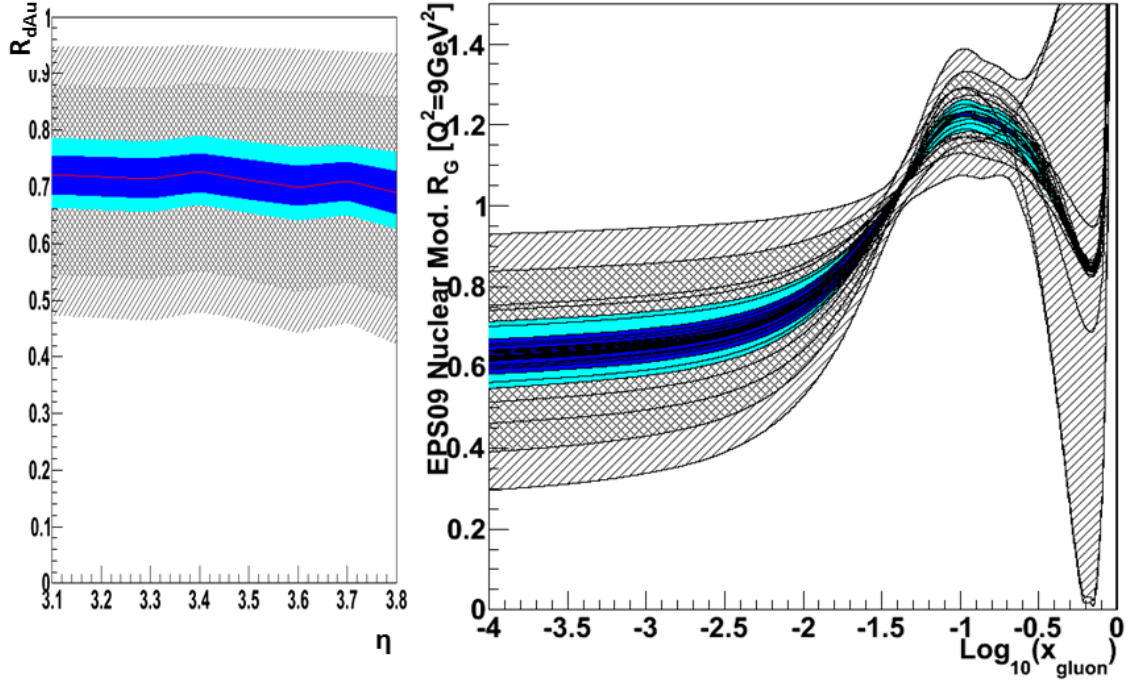
Figure 37: EPS09 exclusion plots in R_{dAu} (left) and R_G (right). The outer hatched lines are the 90% confidence level envelope of all the EPS09 curves. The light blue areas represent the 90% confidence level limits of the simulated measurement, while the dark blue represent the 1σ limits. The nominal value is taken as the central EPS09 curve.

References

[1] A. Adare et al. (PHENIX Collaboration), Direct-Photon Production in p+p Collisions at $\sqrt{s}$ = 200 GeV at Midrapidity, Publication in preparation (2012).

[2] A. Adare et al. (PHENIX Collaboration), Measurement of Direct Photons in Au+Au Collisions at $\sqrt{s}$ = 200 GeV, Publication in preparation (2012).

[3] A. Adare et al. (PHENIX Collaboration), Nuclear effects on direct-photon production in d+Au collisions at $\sqrt{s_{NN}}$=200 GeV, Publication in preparation (2012).

[4] A. Adare et al. (PHENIX Collaboration), Medium Modification of Jet Fragmentation in Au+Au Collisions Measured in Direct Photon-2 Hadron Correlations, Publication in preparation (2012).

[5] A. Adare et al. (PHENIX Collaboration), Y(1S+2S+3S) Production and cold-nuclear-matter effects in d+Au and p+p collisions at $\sqrt{s}$=200 GeV, Publication in preparation (2012).

[6] A. Adare et al. (PHENIX Collaboration), Cold Nuclear Matter Effects on Heavy Quarks and Implications for Energy Loss in the Hot Nuclear Medium from d+Au Collisions at $\sqrt{s}$ = 200 GeV, Publication in preparation (2012).

[7] A. Adare et al. (PHENIX Collaboration), $\frac{dE_T}{d\eta}\big|_{\eta=0}$ as a function of collision centrality for Au+Au collisions at $\sqrt{s_{NN}}$ = 62.4, 130, and 200 GeV, Publication in preparation (2012).

[8] A. Adare et al. (PHENIX Collaboration), J/ψ measurement in Au+Au collisions at $\sqrt{s_{NN}}$ = 200, 62, and 39 GeV, Publication in preparation (2012).

[9] A. Adare et al. (PHENIX Collaboration), Measurement of Transverse Single-Spin Asymmetries for forward-rapidity and midrapidity production of mesons in polarized p+p collisions at $\sqrt{s}$ = 200 and 62 GeV, Publication in preparation (2012).

[10] A. Adare et al. (PHENIX Collaboration), Inclusive cross section and single-transverse-spin asymmetry for very-forward-neutron production in polarized $p + p$ collision at $\sqrt{s}$ = 200 GeV, Publication in preparation (2012).

[11] A. Adare et al. Cross sections and double-helicity asymmetries of midrapidity inclusive charged hadrons in $p + p$ collisions at $\sqrt{s} = 62.4$ GeV. arXiv:1202.4020 [hep-ex] (2012).

[12] A. Adare et al. Deviation from quark-number scaling of the anisotropy parameter v_2 of pions, kaons, and protons in Au+Au collisions at $\sqrt{s_{NN}}$ = 200 GeV. arXiv:1203.2644 [nucl-ex] (2012).

[13] A. Adare et al. Evolution of π^0 suppression in Au+Au collisions from $\sqrt{s_{NN}} = 39$ to 200 GeV. arXiv:1204.1526 [nucl-ex] (2012).

[14] A. Adare et al. Nuclear-Modification Factor for Open-Heavy-Flavor Production at Forward Rapidity in Cu+Cu Collisions at $\sqrt{s_{NN}}$ = 200 GeV. arXiv:1204.0754 [nucl-ex] (2012).

[15] A. Adare et al. Observation of direct-photon collective flow in $\sqrt{s_{NN}}$ = 200 GeV Au+Au collisions. arXiv:1105.4126 [nucl-ex] (2011).

[16] A. Adare et al. Transverse-Momentum Dependence of the J/ψ Nuclear Modification in d+Au Collisions at $\sqrt{s_{NN}}$ = 200 GeV. arXiv:1204.0777 [nucl-ex] (2012).

[17] A. Adare et al. Measurement of bottom versus charm as a function of transverse momentum with electron-hadron correlations in $p+p$ collisions at $\sqrt{s} = 200\,\text{GeV}$. *Phys. Rev. Lett.*, 103:082002, 2009. `arXiv:0903.4851, doi:10.1103/PhysRevLett.103.082002`.

[18] A. Adare et al. Cold Nuclear Matter Effects on J/ψ Yields as a Function of Rapidity and Nuclear Geometry in Deuteron-Gold Collisions at $\sqrt{s_{NN}} = 200$ GeV. *Phys. Rev. Lett.*, 107:142301, 2011. `arXiv:1010.1246, doi:10.1103/PhysRevLett.107.142301`.

[19] A. Adare et al. J/ψ suppression at forward rapidity in Au+Au collisions at $\sqrt{s_{NN}} = 200$ GeV. *Phys. Rev. C*, 84:054912, 2011.

[20] A. Adare et al. Suppression of back-to-back hadron pairs at forward rapidity in d+Au Collisions at $\sqrt{s_{NN}} = 200$ GeV. *Phys. Rev. Lett.*, 107:172301, 2011. `arXiv:1105.5112, doi:10.1103/PhysRevLett.107.172301`.

[21] A. Adare et al. Ground and excited charmonium state production in $p + p$ collisions at $\sqrt{s} = 200\,\text{GeV}$. *Phys. Rev. D*, 85:092004, 2012. `arXiv:1105.1966`.

[22] A. Adil and I. Vitev. Collisional dissociation of heavy mesons in dense-qcd matter. *Physics Letters B*, 649(2-3):139–146, 2007. `doi:10.1016/j.physletb.2007.03.050`.

[23] M. M. Aggarwal et al. Measurement of the parity-violating longitudinal single-spin asymmetry for $w^{\pm}$ boson production in polarized proton-proton collisions at $\sqrt{s} = 500$ *gev*. *Phys. Rev. Lett.*, 106(6):062002, Feb 2011. `doi:10.1103/PhysRevLett.106.062002`.

[24] M. Anselmino, M. Boglione, U. D'Alesio, E. Leader, and F. Murgia. Accessing Sivers gluon distribution via transverse single spin asymmetries in $p\uparrow\ p\ \to\ DX$ processes at RHIC. *Phys. Rev.*, D70:074025, 2004. `arXiv:hep-ph/0407100, doi:10.1103/PhysRevD.70.074025`.

[25] Francois Arleo, Kari J. Eskola, Hannu Paukkunen, and Carlos A. Salgado. Inclusive prompt photon production in nuclear collisions at RHIC and LHC. *JHEP*, 1104:055, 2011. `arXiv:1103.1471, doi:10.1007/JHEP04(2011)055`.

[26] M. A. Betemps, M. B. Gay Ducati, M. V. T. Machado, and J. Raufeisen. Investigating the drell-yan transverse momentum distribution in the color dipole approach. *Phys. Rev. D*, 67:114008, Jun 2003. Available from: `http://link.aps.org/doi/10.1103/PhysRevD.67.114008, doi:10.1103/PhysRevD.67.114008`.

[27] J.D. Bjorken. Highly Relativistic Nucleus-Nucleus Collisions: The Central Rapidity Region. *Phys. Rev.*, D27:140–151, 1983. `doi:10.1103/PhysRevD.27.140`.

[28] A. Capella, L. Bravina, E.G. Ferreiro, A.B. Kaidalov, K. Tywoniuk, et al. Charmonium dissociation and recombination at RHIC and LHC. *Eur. Phys. J.*, C58:437–444, 2008. `arXiv:0712.4331, doi:10.1140/epjc/s10052-008-0772-6`.

[29] A. Capella and E.G. Ferreiro. J/ψ suppression at s**(1/2) = 200-GeV in the comovers interaction model. *Eur. Phys. J.*, C42:419–424, 2005. `arXiv:hep-ph/0505032, doi:10.1140/epjc/s2005-02348-0`.

[30] PHENIX Collaboration. The PHENIX Decadal Plan [online]. 2010. Available from: `http://www.phenix.bnl.gov/phenix/WWW/docs/decadal/2010/phenix_decadal10_full_refs.pdf`.

[31] D. de Florian, R. Sassot, M. Stratmann, and W. Vogelsang. Extraction of Spin-Dependent Parton Densities and Their Uncertainties. *Phys. Rev.*, D80:034030, 2009. `arXiv:0904.3821, doi:10.1103/PhysRevD.80.034030`.

[32] M. Djordjevic, M. Gyulassy, R. Vogt, and S. Wicks. Influence of bottom quark jet quenching on single electron tomography of Au+Au. *Phys. Lett.*, B632:81–86, 2006. `arXiv:nucl-th/0507019, doi:10.1016/j.physletb.2005.09.087`.

[33] Charles Gale. Photon Production in Hot and Dense Strongly Interacting Matter. arXiv:0904.2184 [hep-ph] (2009).

[34] Zhong-Bo Kang, Jian-Wei Qiu, Werner Vogelsang, and Feng Yuan. Accessing tri-gluon correlations in the nucleon via the single spin asymmetry in open charm production. *Phys. Rev.*, D78:114013, 2008. `doi:10.1103/PhysRevD.78.114013`.

[35] Dmitri Kharzeev, Eugene Levin, Marzia Nardi, and Kirill Tuchin. J/ψ production in heavy ion collisions and gluon saturation. *Nucl. Phys.*, A826:230–255, 2009. `arXiv:0809.2933, doi:10.1016/j.nuclphysa.2009.06.016`.

[36] H. Liu, K. Rajagopal, and U. Wiedemann. An AdS/CFT calculation of screening in a hot wind. *Phys. Rev. Lett.*, 98:182301, 2007. `arXiv:hep-ph/0607062, doi:10.1103/PhysRevLett.98.182301`.

[37] S. Turbide, C. Gale, E. Frodermann, and U. Heinz. Electromagnetic radiation from nuclear collisions at RHIC energies. *Phys. Rev.*, C77:024909, 2008. `arXiv:0712.0732, doi:10.1103/PhysRevC.77.024909`.

[38] H. van Hees et al. private communication.

[39] Ivan Vitev and Ben-Wei Zhang. A Systematic study of direct photon production in heavy ion collisions. *Phys. Lett.*, B669:337–344, 2008. `arXiv:0804.3805, doi:10.1016/j.physletb.2008.10.019`.

[40] A. Vossen and others (Belle collaboration). Observation of transverse polarization asymmetries of charged pion pairs in e^+e^- annihilation near $\sqrt{s} = 10.58$ gev. *Phys. Rev. Lett.*, 107:072004, Aug 2011. Available from: `http://link.aps.org/doi/10.1103/PhysRevLett.107.072004`, `doi:10.1103/PhysRevLett.107.072004`.

[41] Bing Zhang, Zhun Lu, Bo-Qiang Ma, and Ivan Schmidt. Extracting boer-mulders functions from $p + d$ drell-yan processes. *Phys. Rev. D*, 77:054011, Mar 2008. Available from: `http://link.aps.org/doi/10.1103/PhysRevD.77.054011`, `doi:10.1103/PhysRevD.77.054011`.

[42] Xingbo Zhao and Ralf Rapp. Charmonium in Medium: From Correlators to Experiment. *Phys. Rev.*, C82:064905, 2010. `arXiv:1008.5328`, `doi:10.1103/PhysRevC.82.064905`.